Approximate coefficient of restitution for nonlinear viscoelastic contact with external load

Abhishek Chatterjee, Guillaume James, Bernard Brogliato

Approximate coefficient of restitution for nonlinear viscoelastic contact with external load

Abhishek Chatterjee[1], Guillaume James[1*] and Bernard Brogliato[1]

[1*]Univ. Grenoble Alpes, INRIA, CNRS, Grenoble INP, LJK, Grenoble, 38000, France.

*Corresponding author(s). E-mail(s): guillaume.james@inria.fr;
Contributing authors: abhishek.chatterjee@inria.fr; bernard.brogliato@inria.fr;

Abstract

We derive an approximate coefficient of restitution (CoR) for a single bead impacting the ground when a constant external load acts upon the colliding body. Some of the main applications concern classical nonlinear viscoelastic models such as the *Kuwabara-Kono* model, *Simon-Hunt-Crossley* model, and Hertzian stiffness with linear damping, however the proposed approach applies to a wide class of nonlinear viscoelastic contact models. It is shown that suitable expansions allow to derive a computable expression of the CoR which provides accurate predictions for a valuable range of external loads, viscosity coefficients and impact velocities.

Keywords: impact, external load, nonlinear viscoelastic contact, coefficient of restitution, analytical approximation

1 Introduction

Impacts in multibody systems are highly nonlinear phenomena whose modelling has attracted numerous researchers since a long time [1–4], see the preface in [5] for a short historical summary. There are several ways to classify impact models within gross classes, as:

1. Single impacts, *i.e.*, a single collision occurs without any overlap with foregoing or next collisions.
2. Multiple impacts, *i.e.*, several collisions occur simultaneously in the system.

or as [6]:

1. Algebraic (zero-order) models which assume instantaneous collisions between perfectly rigid bodies, and relate post- and pre-impact velocities through a so-called restitution rule.
2. First-order dynamics following the Routh and the Darboux-Keller approaches, where the normal contact force impulse is used as a new time-scale.
3. Second-order dynamics which rely on compliant models of lumped flexibilities and dampings (linear or nonlinear spring-dashpot rheological models), through assemblies of various basic components: elastic, viscoelastic, frictional, fractional elastic, viscoplastic, *etc.*

In a Lagrangian framework, simultaneity of collisions means that the boundary of the admissible domain in the configuration space is attained at a co-dimension ≥ 2 submanifold [5, Definition 6.1]. When contact compliance is taken into account, a multiple impact occurs each time several collisions overlap. In this work only single impacts are studied. Each of the above gross classes for single impacts can be refined into subclasses. One

major issue is the modelling of kinetic energy dissipation. Tangential dissipation is usually modelled using extensions of set-valued Coulomb's friction, or tangential coefficients of restitution. As far as normal effects are concerned, several approaches have been proposed so far to take dissipation into account (here we restrict ourselves to single impacts):

1. linear viscosity (damping) [7, 8],
2. nonlinear damping as in the well-known Simon-Hunt-Crossley, Kuwabara-Kono, Tsuji-Tanaka-Ishida models or the Lankarani-Nikravesh approach [9, 10][5, section 2.2.2] [11],
3. phenomenological parameters like coefficients of restitution (CoR) for the zero and first-order dynamics models, the most popular ones being kinematic (Newton), kinetic (Poisson) and energetic CoRs,
4. varying stiffnesses in compression and expansion phases (the bistiffness Crook's approach [12] [5, section 4.2.1.2]) [13],
5. plasticity effects (à la Johnson [14–16] [5, section 4.2.1.1]), Masin, Persoz and viscoelasto-plastic assemblies with set-valued frictional elements [17–19],
6. adhesive effects with Dugdale or Lennard-Jones potentials [20] [5, section 4.2.2], body bulk vibrations (see [1, Chapter III] [15, Chapter 11] [5, section 4.2.4] for references) *etc.*

In addition, it should be remarked that these models and parameters are not independent, nor used independently one from each other. For instance it is known that parameters like CoRs in algebraic restitution rules are related [5, section 4.3.3.1], and this is also the case for first-order Darboux-Keller impact dynamics [21–24] [5, sections 4.3.5.3 and 4.3.6]. Also CoR may be used in rheological models to tune the dissipation parameters as in the Lankarani-Nikravesh approach and its many extensions and variants, see [9, 10] [5, Chapter 2]. Another research direction consists of determining the equivalent CoR to compliant rheological models: the obtained CoR can be used in algebraic models, hence introducing useful informations in the CoR (dependence on pre-impact velocity, on bodies' masses, contact equivalent stiffness, contact equivalent viscous friction, plasticity parameters, contact area, *etc*), while keeping an overall rigid-body instantaneous collisions framework. This is usually not a straighforward task, and it has been the object of many investigations for all types of models, linear spring/dashpots, nonlinear Hertz-plastic piecewise-smooth models [14] [5, section 4.2.1.1] [15], and for nonlinear spring-dashpot Simon-Hunt-Crossley and Kuwabara-Kono models.

A common feature of (almost) all the models and analyses in the literature is that it is assumed, as a fundamental basic assumption, that all the forces which are applied on the colliding bodies at the impact time are negligible compared to the impact forces. Then exact or approximate expressions for the CoR can been derived. This is the case in particular for the Simon-Hunt-Crossley (SHC) [25, 26] and the Kuwabara-Kono (KK) [27] models, which are widely used in applications. Very few studies have analysed the same problem taking into account the effect of an external load on the impacting bodies (*i.e.*, calling into question the fundamental assumption). Among these we may cite [28–31], which all conclude about the importance of considering external loads in certain circumstances. One of the main goals in this article is to study the effect of gravity or constant external force on the computed values of CoR for the Kuwabara-Kono model, thereby extending the fundamental results in [32–35]. The Kuwabara-Kono model stems from continuum mechanics [36–38] and therefore occupies a particular place in the class of rheological compliant spring-dashpot models. The provided theory applies, however, to different viscous nonlinearities than KK, in particular SHC, Hertzian spring with linear dashpot [7], or the Tsuji-Tanaka-Ishida model [11]. Approximate expressions for the CoR are given, and are shown through extensive numerical calculations to fit very well with the exact numerical solution, for a large range of external loads.

The article is organised as follows: the basic model is introduced in section 2. The algorithm for the exact computation of the CoR through the numerical integration of the dynamics is presented in section 3. Section 4 is devoted to the calculation of approximate expressions for the CoR: section 4.1 provides a first order expansion valid for small viscosity coefficients, section 4.2 deals with the case of small equivalent external load, section 4.3 deals with large external loads (and impacts with sticking), the accuracy of the approximation is improved in sections 4.4 and 4.5 by taking

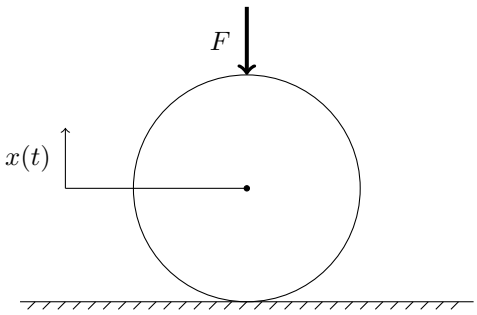

Fig. 1 Single bead impacting ground, with external load

into account high-order terms in the expansions. Section 4.6 compares the analytical approximations of the CoR to the reference values obtained by numerical time integration of the viscoelastic models. Section 5 summarizes the main steps which are needed to calculate the CoR approximations. Conclusions are provided in section 6, and useful calculations can be found in Appendices A, B, and C. Some non-essential components of this work have been skipped in this article, and are presented in the supplementary technical report [39].

2 Nonlinear viscoelastic impact model

Consider a system consisting of a single bead impacting the ground, as shown in Fig. 1. The mass of the bead is m and the stiffness constant is k. The external load induced on the bead is given by the parameter F, such that $F > 0$ produces a compressive (downward) force on the bead according to Fig. 1. The external load F is considered to be constant, which is a realistic assumption given that impact duration is typically very small. The displacement of the center of the bead in reference to the undeformed position is denoted by $x(t)$, such that the bead is in contact when $x(t) \leq 0$ and free when $x(t) > 0$. Then, based on a general viscoelastic model, the equation of motion of the bead is given by

$$m\ddot{x} = k\left[(-x)_+^\alpha + \gamma_0 \frac{d}{dt}(-x)_+^\beta\right] - mg - F, \quad (1)$$

where $x_+ = \max(x, 0)$. The initial conditions for (1) are $x(0) = 0$ and $\frac{dx}{dt}(0) = -v_0$ with $v_0 > 0$. The parameters $\alpha > 0$, $\beta > 0$ and $\gamma_0 \geq 0$ characterize the contact force behaviour: α is associated with the stiffness, whereas β and γ_0 control the dissipation during the impact. In this study, we make the following assumption which guarantees that the dynamical equations are sufficiently smooth (at least Lipschitz continuous, see equation (6) below).

Assumption 1 *$\alpha \geq 1$ and $\beta \geq 1$.*

If the parameter values are chosen to be $\alpha = \beta = \frac{3}{2}$, the viscoelastic model (1) is known as the Kuwabara-Kono model [27], similarly if $\alpha = 3/2$ and $\beta = 5/2$, the Simon-Hunt-Crossley model [25, 26] is obtained. The case $\alpha = 3/2$ and $\beta = 1$ corresponds to Hertz contact with linear damping. In this work we will pay particular attention to these cases in numerical simulations, while our analytical study of the impact model (1) will be performed under the general assumption 1. The dynamics of (1) can be rescaled with respect to the time and length scales:

$$T = \left(\tfrac{m}{k}\right)^{\frac{1}{\alpha+1}} v_0^{\frac{1-\alpha}{\alpha+1}} \qquad \text{and } \delta = v_0 T$$

by setting $x(t) = -\delta u(\tau)$ with $\tau = \frac{t}{T}$. Then the scaled dynamics is given by

$$\frac{d^2u}{d\tau^2} + \gamma \frac{d}{d\tau}\left(u_+^\beta\right) + u_+^\alpha = \tilde{g}, \quad (2)$$

where

$$\gamma = \gamma_0 v_0^{\frac{2\beta}{\alpha+1}-1}\left(\frac{k}{m}\right)^{1-\frac{\beta}{\alpha+1}}, \quad (3)$$

and

$$\tilde{g} = \left(g + \frac{F}{m}\right)\frac{T^2}{\delta} = \left(\frac{m}{k}\right)^{\frac{1}{\alpha+1}} v_0^{\frac{-2\alpha}{\alpha+1}}\left(g + \frac{F}{m}\right). \quad (4)$$

The initial conditions for the scaled equations of motion (2) are $u(0) = 0$ and $\frac{du}{d\tau}(0) = 1$.

The dimensionless parameters γ (rescaled dissipation constant) and $\tilde{g}$ (rescaled external force) both depend on the impact velocity v_0, and $\tilde{g}$ also depends on the external load F, as illustrated in Fig. 2 for the Kuwabara-Kono model ($\alpha = \beta = 3/2$). Figure 2(a) shows the relationship between γ and the initial velocity v_0, where we can see that γ increases with v_0 since $\beta > (\alpha + 1)/2$ in the Kuwabara-Kono model. Figure 2(b) shows

$\tilde{g}$ versus the external load F, for different values of v_0. Here we see that the specific value $F = -mg$ balances the gravitational constant, and that decreasing the initial velocity v_0 increases the magnitude of the rescaled external force $\tilde{g}$, which diverges in the limit of vanishing impact velocity.

Let us assume that the impact terminates at $\tau = T_f > 0$. The impact takes place for $\tau \in (0, T_f)$, so the scaled displacement $u(\tau)$ is positive while $\tau \in (0, T_f)$ and $u(T_f) = 0$ at impact termination. The CoR for the impact can be expressed in terms of the scaled velocities as

$$e = -\frac{\frac{du}{d\tau}(T_f)}{\frac{du}{d\tau}(0)} = -\frac{du}{d\tau}(T_f). \tag{5}$$

Thus, the CoR for a given impact can be numerically evaluated by integrating the ordinary differential equation for the scaled dynamics given in (2) until $\tau = T_f$.

Note that the vanishing of the contact force is sometimes used as an alternative condition for the end of collision, in order to avoid an attractive contact force near contact breaking when $\gamma > 0$ and $\beta < \alpha + 1$ (see e.g. [35]). In this work, we restrict ourselves to the classical condition of vanishing bead deformation $u(T_f) = 0$, and we derive analytical approximations of the CoR (5) for $\alpha, \beta \geq 1$ and a valuable range of dimensionless parameters γ and $\tilde{g}$. The CoR obtained through numerical integration of (2) will serve as a reference to assess the validity of the analytical approximations. The next section discusses the method used for numerically integrating (2).

3 Calculation of the CoR by numerical time integration

The term $\frac{d}{d\tau}\left(u_+^\beta\right) = \beta\, u_+^{\beta-1}\, \frac{du}{d\tau}$ in (2) is not Lipschitz continuous for $\beta < 2$ and therefore can create difficulty with the numerical integration. As discussed in [40, 41], these issues can be circumvented with an appropriate choice of the dynamical variable. Hence, here we will consider the same change of variable, and rewrite (2) in terms of a new *generalized velocity* variable w:

$$\begin{aligned} \frac{du}{d\tau} &= w - \gamma u_+^\beta, \\ \frac{dw}{d\tau} &= -u_+^\alpha + \tilde{g}, \end{aligned} \tag{6}$$

with the initial condition $u(0) = 0$ and $w(0) = 1$, which implies $u'(0) = 1$.

Solutions of (6) are computed for $\gamma \geq 0$ and $\tilde{g} \geq 0$. Time integration is performed using the `ode45` solver of `MATLAB` (with absolute and relative error tolerances set to 10^{-14} and 10^{-10}). The dynamical equations have to be numerically integrated up to $\tau = T_f$ to obtain the CoR of the bead, and the value of T_f is not a priori known. Whether the impact terminates or not depends on the parameter values α, β, γ and $\tilde{g}$.

If the impact terminates, the bead detaches at some time T_f such that $u(T_f) = 0$ and $u'(T_f) \in [-1, 0)$, which leads $e = -u'(T_f) \in (0, 1]$. This case is illustrated in Figure 3 for $\alpha = \beta = 3/2$, $\gamma = 0.006$ and $\tilde{g} = 0.1$. If $\tilde{g} > 0$, additional collisions will occur for $\tau > T_f$ but we do not compute the solution in this time domain. Similarly, we do not examine the convergence of $u(\tau)$ towards the equilibrium $\bar{u} = \tilde{g}^{\frac{1}{\alpha}}$ that occurs for $\gamma > 0$ and $\tilde{g} > 0$ when $\tau \to +\infty$.

If the bead does not detach after the initial impact, one has $u(\tau) \geq 0$ for all $\tau \geq 0$, and $\lim_{\tau \to +\infty} u(\tau) = \bar{u}$ since necessarily $\gamma > 0$. In that case, the CoR of the bead is $e = 0$ and time integration will be stopped when (u, u') becomes very close to $(\bar{u}, 0)$. Note that the interval of time integration can be reduced when the convergence towards equilibrium occurs with oscillations, as illustrated in Fig. 4 ($\alpha = \beta = 3/2$, $\gamma = 0.06$ and $\tilde{g} = 4$). Indeed, one can stop time integration if $u(T_f) \in [0, \bar{u}]$ and $u'(T_f) = 0$, since we have then $u(t) \geq u(T_f) \geq 0$ for all $t \geq T_f$ and convergence to equilibrium occurs.

In summary, time integration is stopped at $t = T_f > 0$ either when $u(T_f)u'(T_f) = 0$ with $u(T_f) \in [0, \bar{u}]$ (then $e = -u'(T_f)$), or when $\|(u - \bar{u}, u')(T_f)\|_\infty < \varepsilon$, for some small threshold ε (we fix $\varepsilon = 10^{-8}$), leading to $e = 0$.

Note that for $\tilde{g} > 0$, the transition from the situation of Fig. 3 ($e \in (0, 1]$) to the case of Fig. 4 ($e = 0$) occurs when $u(T_f) = u'(T_f) = 0$ for a critical damping constant $\gamma_c > 0$, and the CoR

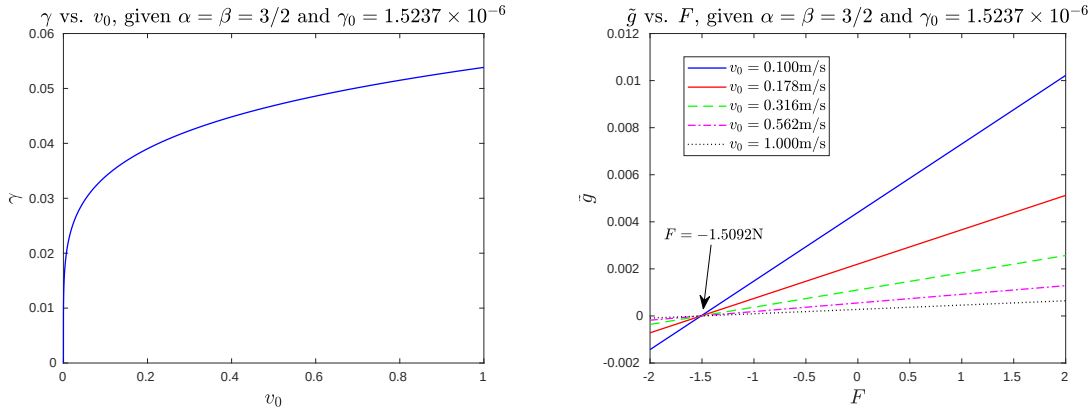

Fig. 2 Values of the dimensionless parameters γ and $\tilde{g}$ versus (a) initial velocity v_0 and (b) external load F, for the Kuwabara-Kono model ($\alpha = \beta = 3/2$). The gravitational constant is $g = 9.8\text{m/s}^2$. Values for mass $m = 1.54 \times 10^{-1}$kg and stiffness $k = 3.6138{\times}10^{10}\text{N/m}^{3/2}$ are taken from [27] (impacts of steel balls) and the dissipation constant $\gamma_0 = 1.5237{\times}10^{-6}$s is calculated using the CoR $e = 0.893$ reported in [27], according to the method described in [40] for approximating γ versus e.

is a continuous decreasing function of γ vanishing for $\gamma \geq \gamma_c$.

4 Analytical CoR approximations

The main goal of the paper is addressed in this section, where we derive a hierarchy of analytical approximations of the CoR, and compare them to numerical computations as described in the previous section. Henceforth we denote by an *approximation of order p* of the CoR $e(\gamma)$, or $\mathcal{O}(\gamma^p)$ approximation, an approximation whose Taylor expansion at $\gamma = 0$ is correct up to order p. Section 4.1 introduces a $\mathcal{O}(\gamma)$ approximation and sections 4.2, 4.3 examine its simplifications when $\tilde{g}$ is either small or large. Sections 4.4 and 4.5 deal with $\mathcal{O}(\gamma^2)$ approximations.

4.1 First order approximation of the CoR for small γ

In this section we derive a first order approximation of the CoR e when $\gamma \approx 0$. Multiplying the equations of motion (2) by $\frac{du}{d\tau}$ gives for $u \geq 0$

$$\frac{d}{d\tau}\left[\frac{1}{2}\left(\frac{du}{d\tau}\right)^2\right] + \gamma\beta\left(\frac{du}{d\tau}\right)^2 u^{\beta-1} + \frac{d}{d\tau}\left(\frac{u^{\alpha+1}}{\alpha+1}\right) = \tilde{g}\frac{du}{d\tau}, \tag{7}$$

which if integrated from $\tau = 0$ to $\tau = T_f$ yields

$$e^2 = 1 - 2\gamma\beta\int_0^{T_f}\left(\frac{du}{d\tau}\right)^2 u^{\beta-1}d\tau. \tag{8}$$

This identity expresses the contribution of dissipative terms of (2) to the decrease of the coefficient of restitution e.

Let us now consider the scaled displacement $u_0(\tau)$ and time of detachment T_0 corresponding to the non-dissipative case $\gamma = 0$, in which equation (2) reads

$$\frac{d^2u_0}{d\tau^2} + u_0^\alpha = \tilde{g}, \tag{9}$$

with

$$u_0(0) = 0, \quad \frac{du_0}{d\tau}(0) = 1,$$

$$u_0(T_0) = 0, \quad \frac{du_0}{d\tau}(T_0) = -1.$$

Now assuming $\gamma \approx 0$, we have $u(\tau) = u_0(\tau) + \mathcal{O}(\gamma)$ and $T_f = T_0 + \mathcal{O}(\gamma)$. Consequently, equation (8) can be expanded as

$$e^2 = 1 - 2\gamma\beta\mathcal{I}_0(\tilde{g}) + \text{H.O.T.}, \tag{10}$$

where

$$\mathcal{I}_0(\tilde{g}) = \int_0^{T_0}\left(\frac{du_0}{d\tau}\right)^2 u_0^{\beta-1}d\tau. \tag{11}$$

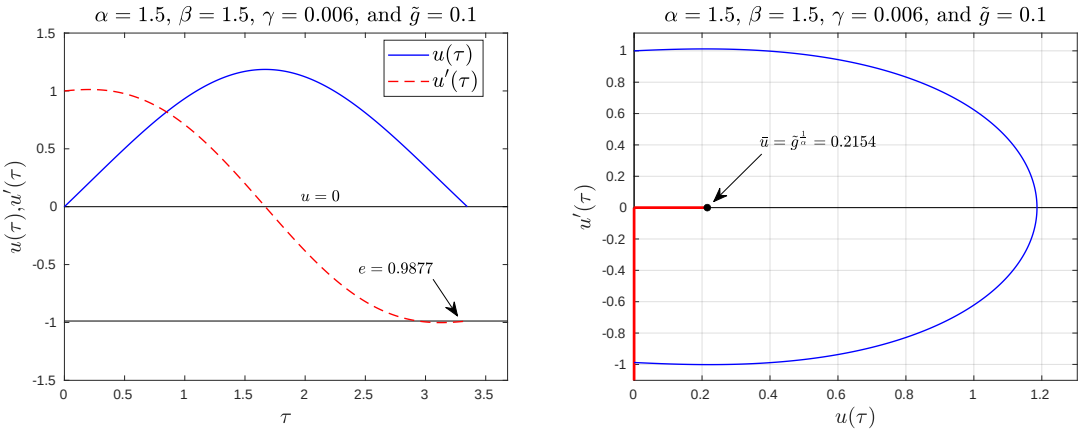

Fig. 3 Numerical integration of scaled dynamics for the parameters $\alpha = \beta = \frac{3}{2}$, $\gamma = 0.006$ and $\tilde{g} = 0.1$: (a) Graphs of $u(\tau)$ and $u'(\tau)$, and (b) Phase-space plot of $(u(\tau), u'(\tau))$ (the stopping condition is shown in red). The bead detaches when $u(\tau)$ vanishes with $u'(\tau) < 0$, leading to $e \in (0, 1)$.

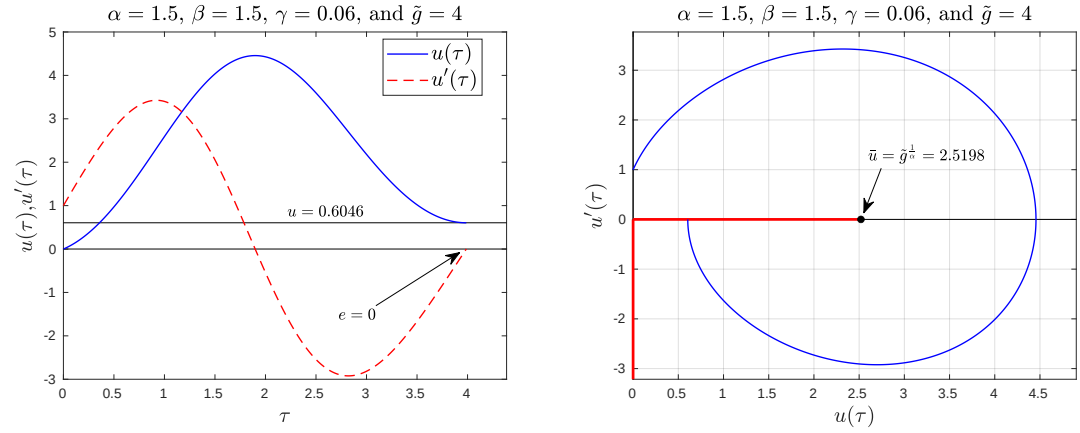

Fig. 4 Numerical integration of scaled dynamics for the parameters $\alpha = \beta = \frac{3}{2}$, $\gamma = 0.06$ and $\tilde{g} = 4$: (a) Graphs of $u(\tau)$ and $u'(\tau)$, and (c) Phase-space plot of $(u(\tau), u'(\tau))$ (the stopping condition in shown in red). The bead does not detach and time integration terminates when $0 < u(\tau) < \tilde{g}^{\frac{1}{\alpha}}$ and $u'(\tau) = 0$, leading to $e = 0$.

We show in appendix A that

$$\mathcal{I}_0(\tilde{g}) = 2\int_0^{u_M} \left[1 + 2\left(\tilde{g}u_0 - \frac{{u_0}^{\alpha+1}}{\alpha+1}\right)\right]^{\frac{1}{2}} u_0^{\beta-1} du_0, \tag{12}$$

where $u_M = u_0\left(\frac{T_0}{2}\right)$ is the maximal compression in the absence of dissipation and satisfies

$$\frac{1}{\alpha+1}{u_M}^{\alpha+1} - \tilde{g}u_M = \frac{1}{2}. \tag{13}$$

Based on (13), we can observe that the maximal compression u_M depends on $\tilde{g}$ (henceforth we shall refer to $u_M(\tilde{g})$ when using this dependency). In particular, the maximal compression u_M^* in the absence of external load is given by

$$u_M^* = u_M(0) = \left(\frac{\alpha+1}{2}\right)^{\frac{1}{\alpha+1}}. \tag{14}$$

Taking the square root of both sides of (10), one obtains the following first order expansion for

small γ

$$e = 1 - \gamma\,\beta\,\mathcal{I}_0(\tilde{g}) + \text{H.O.T.}, \tag{15}$$

where the integral $\mathcal{I}_0(\tilde{g})$ is given by (12). An exact closed-form expression is unknown for this integral, but in the following sections we will introduce a number of analytical approximations (asymptotic behavior for small or large $\tilde{g}$, and approximation by a quadrature formula based on Chebyshev interpolation for arbitrary $\tilde{g}$).

4.2 CoR approximation for small $\tilde{g}$

We begin by approximating e for $\tilde{g} \approx 0$, and perform a first-order Taylor expansion of (15) about $\tilde{g} = 0$,

$$e = 1 - \gamma\beta\mathcal{I}_0(0) - \gamma\beta\tilde{g}\frac{d\mathcal{I}_0}{d\tilde{g}}(0) + \text{H.O.T.} \tag{16}$$

Using Leibniz integral rule and equation (13), one obtains

$$\frac{d\mathcal{I}_0}{d\tilde{g}} = 2\int_0^{u_M}\left[1 + 2\left(\tilde{g}u_0 - \frac{u_0^{\alpha+1}}{\alpha+1}\right)\right]^{-\frac{1}{2}} u_0^{\beta} du_0. \tag{17}$$

Setting $\tilde{g} = 0$ in (12) and (17) and using (14), expansion (16) finally reads

$$e = 1 - \gamma C_0 - \gamma\,\tilde{g}C_1 + \text{H.O.T.}, \tag{18}$$

with

$$C_0 = \beta\,\mathcal{I}_0(0) = 2\beta\int_0^{u_M^*}\left[1 - 2\frac{{u_0}^{\alpha+1}}{\alpha+1}\right]^{\frac{1}{2}} {u_0}^{\beta-1} du_0,$$

$$C_1 = \beta\,\frac{d\mathcal{I}_0}{d\tilde{g}}(0) = 2\beta\int_0^{u_M^*}\left[1 - 2\frac{{u_0}^{\alpha+1}}{\alpha+1}\right]^{-\frac{1}{2}} {u_0}^{\beta} du_0.$$

We can notice that the definite integrals C_0 and C_1 can be rewritten in the form of *Euler's Beta Function*

$$\mathrm{B}(z,w) = \int_0^1 t^{z-1}(1-t)^{w-1}dt$$

which is defined for $w, z > 0$. Indeed, for all $x, y, \rho, \lambda \in \mathbb{R}$ with $\rho, \lambda > 0$ and $x, y > -1$, the following identity holds true

$$\int_0^{(1/\rho)^{1/\lambda}} t^x\left(1 - \rho t^{\lambda}\right)^y dt = \frac{1}{\lambda\rho^{(x+1)/\lambda}}\mathrm{B}\left(\frac{x+1}{\lambda}, y+1\right). \tag{19}$$

Using the upper bound (14) of the integrals C_0, C_1 and identity (19), we find

$$C_0 = \beta\left(\frac{\alpha+1}{2}\right)^{\frac{\beta-\alpha-1}{\alpha+1}}\mathrm{B}\left(\frac{\beta}{\alpha+1}, \frac{3}{2}\right),$$

$$C_1 = \beta\left(\frac{\alpha+1}{2}\right)^{\frac{\beta-\alpha}{\alpha+1}}\mathrm{B}\left(\frac{\beta+1}{\alpha+1}, \frac{1}{2}\right). \tag{20}$$

Note that expansion (18) with the coefficient C_0 given in (20) was previously derived in [42] for $\tilde{g} = 0$ and $\alpha = 3/2$ (see also [28]).

Next, having obtained the first-order analytical approximation (18) of e for small values of γ and $\tilde{g}$, we will study the validity of this approximation against numerical time integration of (6) as described in section 3.

Figure 5 compares the CoR values computed using approximation (18) and the values obtained through numerical time integration, for $\alpha = \beta = 3/2$, $\tilde{g} \in [0, 10]$ and $\gamma = 10^{-4}, 10^{-3}, 10^{-2}$ from top to bottom. The approximate CoR (18) works well for $\tilde{g}$ small enough, for example close to the value $\tilde{g}_0 = 5.1224 \times 10^{-4}$ obtained using parameters from [43] (see the zoomed plots in panels 5(b)-(d)-(f)). However one needs a better approximation for larger values of $\tilde{g}$. In particular, in Fig. 5(e) the numerically calculated CoR vanishes above a critical value $\tilde{g} \approx 3.7$ (absence of bead detachment), a phenomenon which is not accurately captured by approximation (18).

In order to understand the connection between the value of γ and the value of $\tilde{g}$ beyond which the bead doesn't detach, we will derive in the next section an approximation of the CoR adapted to the case of large $\tilde{g}$.

4.3 CoR approximation for large $\tilde{g}$ and no-detachment condition

As seen in the previous section, it is relatively straightforward to derive an analytical approximation of the CoR for small values of $\tilde{g}$. However this approximation becomes highly inaccurate when $\tilde{g}$

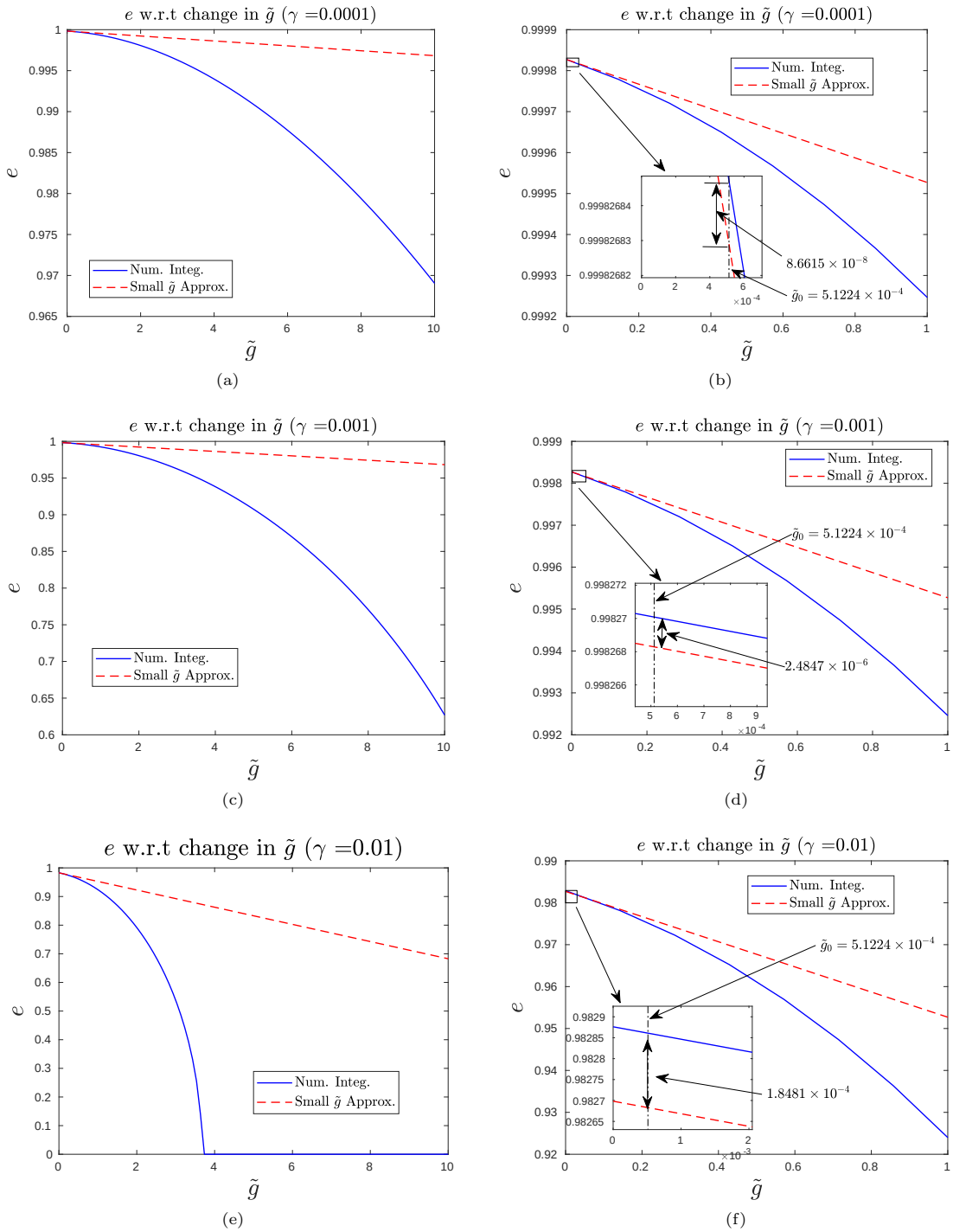

Fig. 5 Change in CoR with respect to $\tilde{g} \in [0, 10]$ (left panels (a)-(c)-(e)) and $\tilde{g} \in [0, 1]$ (right panels (b)-(d)-(f)), with zoomed plots around $\tilde{g} = \tilde{g}_0 = 5.1224 \times 10^{-4}$ (value calculated using parameters from [43], for a 8mm diameter steel bead with $m = 2.05 \times 10^{-3}$kg, $k = 6.9716 \times 10^{9}\text{N/m}^{\frac{3}{2}}$, $v_0 = 0.246$m/s, $g = 9.8\text{m/s}^2$, and $F = 0$N). The other parameters are $\alpha = \beta = \frac{3}{2}$ and $\gamma = 0.0001$ (top panels (a)-(b)), $\gamma = 0.001$ (middle panels (c)-(d)), $\gamma = 0.01$ (bottom panels (e)-(f)). The numerically computed values of CoR are labelled *Num. Integ.* and the values obtained using approximation (18) are labeled *Small $\tilde{g}$ Approx.*

becomes large, hence a different CoR approximation is needed in this case.

In Appendix A, we derive from (10) for $\tilde{g} \gg 1$ the following expansion of the squared CoR

$$e^2 \approx 1 - 2\gamma C \tilde{g}^{\left(\frac{\beta}{\alpha}+\frac{1}{2\alpha}+\frac{1}{2}\right)}, \tag{21}$$

with

$$C = 2\sqrt{2}\frac{\beta}{\alpha}(\alpha+1)^{\left(\frac{\beta}{\alpha}+\frac{1}{2\alpha}\right)}\mathrm{B}\left(\frac{\beta+1/2}{\alpha}, \frac{3}{2}\right).$$

It is clear from (21) that the CoR e decreases as $\tilde{g}$ increases. Moreover, for $\alpha, \beta \geq 1$ and small $\gamma > 0$, there exists $\tilde{g}_c \gg 1$ satisfying

$$\tilde{g}_c^{\left(\frac{\beta}{\alpha}+\frac{1}{2\alpha}+\frac{1}{2}\right)} \approx \frac{1}{2\gamma C}, \tag{22}$$

such that $e = 0$ for $\tilde{g} = \tilde{g}_c$ and $e > 0$ when $1 \ll \tilde{g} < \tilde{g}_c$.

Of course approximation (21) is only valid when the right side is nonnegative, i.e. for $\tilde{g} \leq \tilde{g}_c$ when $\gamma > 0$. An interpretation of this condition is that when $\tilde{g} \geq \tilde{g}_c$, the assumption of impact termination is violated, i.e. the bead sticks to the ground. This interpretation is consistent with our numerical simulations, where we observe that the bead does not detach if $\gamma > 0$ is fixed and $\tilde{g}$ chosen large enough, as illustrated in Fig. 5(e). Therefore, using (22) one can approximate the smallest value $\tilde{g}_c$ of $\tilde{g}$ beyond which the CoR will remain zero. For example, for the Kuwabara-Kono model ($\alpha = \beta = 3/2$), one finds $C = 5\sqrt{2}(5/2)^{1/3}\mathrm{B}\,(4/3, 3/2) \approx 4.403986$ which yields $\tilde{g}_c \approx 0.30522\,\gamma^{-6/11}$. Equivalently, for a given value of $\tilde{g}$, (21) can also be used to approximate the smallest value γ_c of γ above which $e = 0$,

$$\gamma_c \approx \frac{1}{2C}\,\tilde{g}^{-\left(\frac{\beta}{\alpha}+\frac{1}{2\alpha}+\frac{1}{2}\right)}.$$

Condition (22) can work for any value of $\alpha, \beta \geq 1$. Figure 6 presents three different cases corresponding to $\alpha = 3/2$ and $\beta = 1$ (Hertz stiffness with linear damping, top panels), $\beta = 3/2$ (Kuwabara-Kono model, middle panels) and $\beta = 5/2$ (Simon-Hunt-Crossley model, bottom panels). Fig. 6(a)-(c)-(e) show the dependence of $\tilde{g}_c$ on $\gamma \in (0, 1]$. The analytical approximation (22) of $\tilde{g}_c$ is compared to its numerical values obtained by time integration of the dynamical equations (using the bisection method to find the value of $\tilde{g}$ that cancels the CoR). Fig. 6(b)-(d)-(f) show the relative errors of the analytical approximation with respect to numerically computed values.

We can see from Fig. 6 that when γ is small enough, the analytical approximation (22) of $\tilde{g}_c \gg 1$ closely matches the numerically computed values (see the zoomed plots for $\gamma \in (0, 0.01]$). This also confirms that the analytical approximation of e for large values of $\tilde{g}$ given by (21) is correct. However, the analytical approximation of $\tilde{g}_c$ becomes imprecise when γ increases, as shown in Fig. 6(b)-(d)-(f).

Whereas the CoR approximations derived so far linearly depend on γ, higher order terms would be useful to increase their range of validity and describe the vanishing of the CoR in parameter regimes where $\tilde{g}$ is not too large. In the next section, we will derive additional approximations of e that include an $\mathcal{O}(\gamma^2)$ term and can work in a larger parameter range.

4.4 CoR approximations including an $\mathcal{O}(\gamma^2)$ term

In order to make the CoR approximation valid over larger ranges of γ and $\tilde{g}$, we need to include higher-order terms in the expansion. In this section we will introduce an additional $\mathcal{O}(\gamma^2)$ term leading to a CoR approximation of the form

$$e = 1 - \gamma C_0 - \gamma \tilde{g} C_1 - \gamma^2 C_2 + \text{H.O.T.}, \tag{23}$$

where C_0 and C_1 are the coefficients obtained in (18)-(20) and the quadratic coefficient C_2 needs to be determined. Approximation (23) corresponds to the second order Taylor expansion of $e(\gamma, \tilde{g})$ at $(\gamma, \tilde{g}) = (0, 0)$. In section 4.4.1, we will consider the expansion obtained by Schwager and Pöschel [32, 35] for the Kuwabara - Kono model ($\alpha = \beta = 3/2$) with no external force ($\tilde{g} = 0$). Incorporating this $\mathcal{O}(\gamma^2)$ correction term, we will evaluate the departure of the new analytical approximation from the numerically computed CoR.

In section 4.4.2, we will derive a more general $\mathcal{O}(\gamma^2)$ expansion of e in terms of γ, valid for all values of $\tilde{g}$ and $\alpha, \beta \geq 1$,

$$e = 1 - A_1(\tilde{g})\,\gamma - A_2(\tilde{g})\,\gamma^2 + \text{H.O.T.}, \tag{24}$$

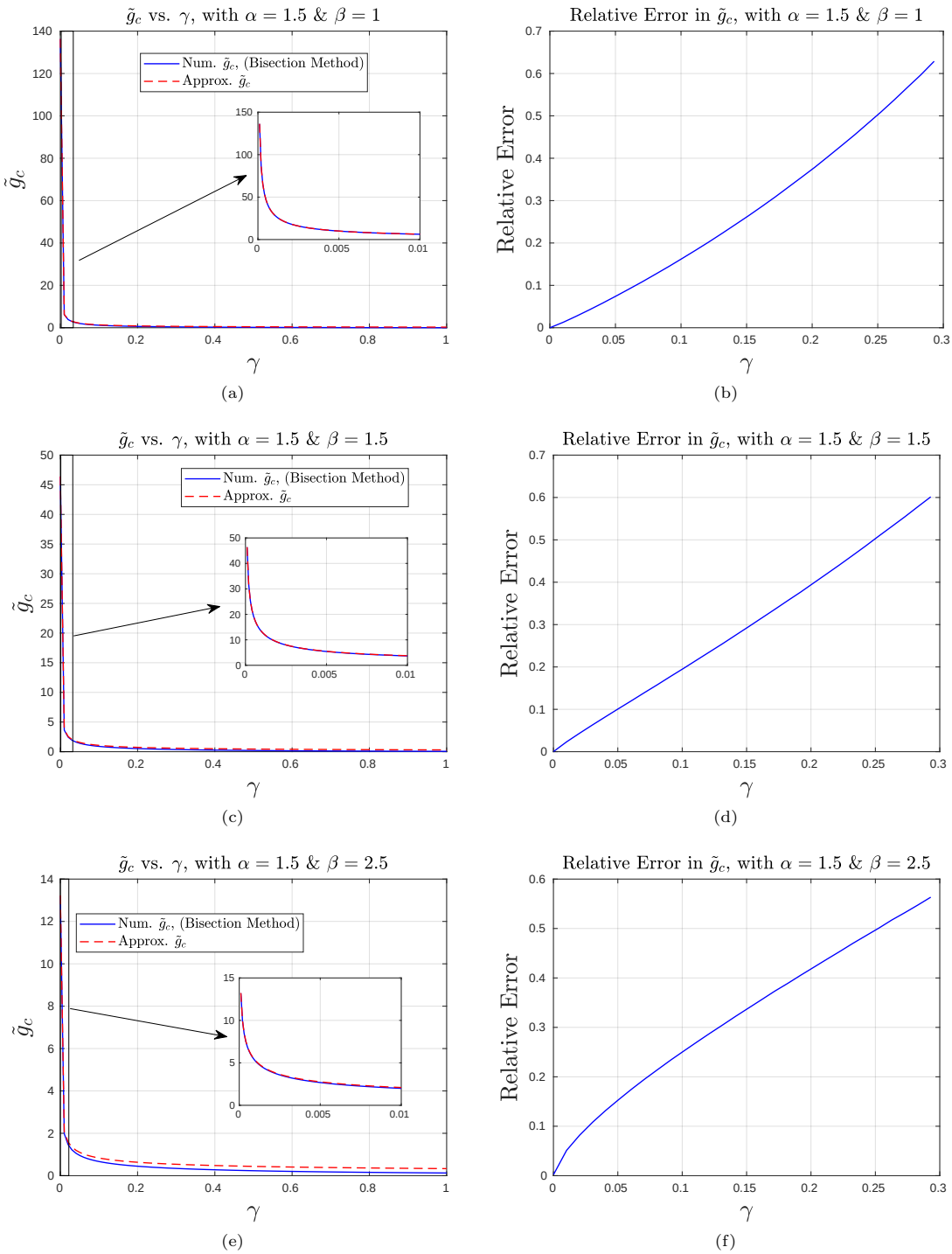

Fig. 6 Critical value $\tilde{g}_c$ of the rescaled external force above which the bead sticks to the ground, plotted versus the rescaled dissipation constant $\gamma \in (0, 1]$ (left panels (a)-(c)-(e)), for $\alpha = 3/2$ (zoomed plots with $\gamma \in (0, 0.01]$ are included). Top panels correspond to $\beta = 1$ (Hertz stiffness and linear damping), middle panels to $\beta = 3/2$ (Kuwabara-Kono model) and bottom panels to $\beta = 5/2$ (Simon-Hunt-Crossley model). Plots labeled *Num. $\tilde{g}_c$ (Bisection Method)* refer to the numerical values obtained by time integration of the dynamical equations, using the bisection method to find the value of $\tilde{g}$ that cancels the CoR. Plot labeled *Approx. $\tilde{g}_c$* correspond to the analytical approximation (22). Right panels (b)-(d)-(f) display relative errors between the analytical approximation of $\tilde{g}_c$ and the numerically computed values for $\gamma \in (0, 0.3]$.

without linearizing the CoR with respect to $\tilde{g}$ (even though the linearized expansion (23) will be obtained as a byproduct for all $\alpha, \beta \geq 1$). However, the coefficients A_1, A_2 will be defined by integrals which cannot be explicitly computed even in terms of special functions (unlike the coefficients C_i calculated using Euler's Beta function). This will motivate further approximations discussed in section 4.5.

4.4.1 The Schwager-Pöschel CoR approximation

The CoR approximation obtained by Schwager and Pöschel [35] is a power-series expansion of e with respect to γ, assuming no external force ($\tilde{g} = 0$) and $\alpha = \beta = \frac{3}{2}$. In this work we are only concerned with the expansion involving terms up to $\mathcal{O}(\gamma^2)$, which as per [35] (Eq. (36) and Table III) is given by

$$e = 1 + a\,\mu\, v_0^{\frac{1}{5}} + b\,\mu^2 v_0^{\frac{2}{5}} + \text{H.O.T.}, \tag{25}$$

where v_0 is the pre-impact velocity,

$$a = -1.153448854, \quad b = 0.7982665553, \tag{26}$$

$$\mu = \frac{3}{2}\gamma_0 \left(\frac{k}{m}\right)^{\frac{2}{5}}.$$

Using (3) for $\alpha = \beta = \frac{3}{2}$, we obtain $\gamma = \gamma_0 v_0^{\frac{1}{5}} \left(\frac{k}{m}\right)^{\frac{2}{5}}$, hence we have $\mu = \frac{3}{2}\gamma v_0^{-\frac{1}{5}}$ and (25) becomes

$$e = 1 + \frac{3}{2}a\,\gamma + \frac{9}{4}b\,\gamma^2 + \text{H.O.T.} \tag{27}$$

Comparing (27) with (23) for $\tilde{g} = 0$, we notice that

$$C_0 = -\frac{3}{2}a, \quad C_2 = -\frac{9}{4}b, \tag{28}$$

and thus

$$C_0 = 1.730173281, \quad C_2 = -1.7960997494. \tag{29}$$

Expression (20) evaluated for $\alpha = \beta = \frac{3}{2}$ yields $C_0 = 1.730173287142$ which agrees well with (29).

Having now determined the value of C_2 in the expansion (23) for $\alpha = \beta = \frac{3}{2}$, we will study the effect of the corresponding $\mathcal{O}(\gamma^2)$ term in the approximation.

Figure 7 shows how e varies with respect to $\gamma \in [0, 0.1]$, for fixed values of $\tilde{g} = 0$, 0.05, 1 and 10. The CoR obtained via numerical integration of (6) is compared to the first-order approximation (18) and the $\mathcal{O}(\gamma^2)$ approximation (23). The corresponding absolute errors are displayed in Figure 8.

We observe that the inclusion of the $\mathcal{O}(\gamma^2)$ term improves the accuracy of the approximation of e when $\tilde{g} = 0$ (Fig. 7(a) and Fig. 8(a)), and for $0 < \tilde{g} \ll 1$ with γ not too small (Fig. 7(b) and Fig. 8(b)). However, both approximations (18) and (23) fail when $\tilde{g}$ is further increased (Fig.7(c)-(d) and Fig. 8(c)-(d)). This is due to the fact that these approximations are derived by perturbation for $\tilde{g} \approx 0$. In the following section, we will derive a CoR expansion of the form (24) valid for arbitrary $\tilde{g}$.

4.4.2 CoR expansion for small γ and arbitrary $\tilde{g}$

In this section, we derive an $\mathcal{O}(\gamma^2)$ expansion of the CoR e of the form (24) valid for arbitrary values of $\tilde{g}$ and $\alpha, \beta \geq 1$. This will allow us to accurately approximate the CoR over a wider parameter range compared to previous approximations valid for $\tilde{g} \approx 0$ (expansion (23) derived for $\alpha = \beta = 3/2$ and expansion(18)).

We begin by considering u as a function of (γ, τ), and consider equation (2) for $u \geq 0$,

$$\frac{\partial^2 u}{\partial \tau^2} + \gamma \frac{\partial}{\partial \tau}\left(u^\beta\right) + u^\alpha = \tilde{g}, \tag{30}$$

with

$$u(\gamma, 0) = 0 \text{ and } \frac{\partial u}{\partial \tau}(\gamma, 0) = 1, \tag{31}$$

where $\tau \in [0, T_f]$, T_f is the impact duration with $u(\gamma, T_f) = 0$ and $\frac{\partial u}{\partial \tau}(\gamma, T_f) = -e$. The task at hand is to expand the CoR with respect to $\gamma \approx 0$ using identity (8), namely

$$\begin{aligned} e^2 &= 1 - 2\gamma\beta\mathcal{I}(\gamma, \tilde{g}), \\ \mathcal{I}(\gamma, \tilde{g}) &= \int_0^{T_f} \left(\frac{\partial u}{\partial \tau}\right)^2 u^{\beta-1} d\tau. \end{aligned} \tag{32}$$

The integral function $\mathcal{I}(\gamma, \tilde{g})$ can be simplified, by first performing an integration by parts and then

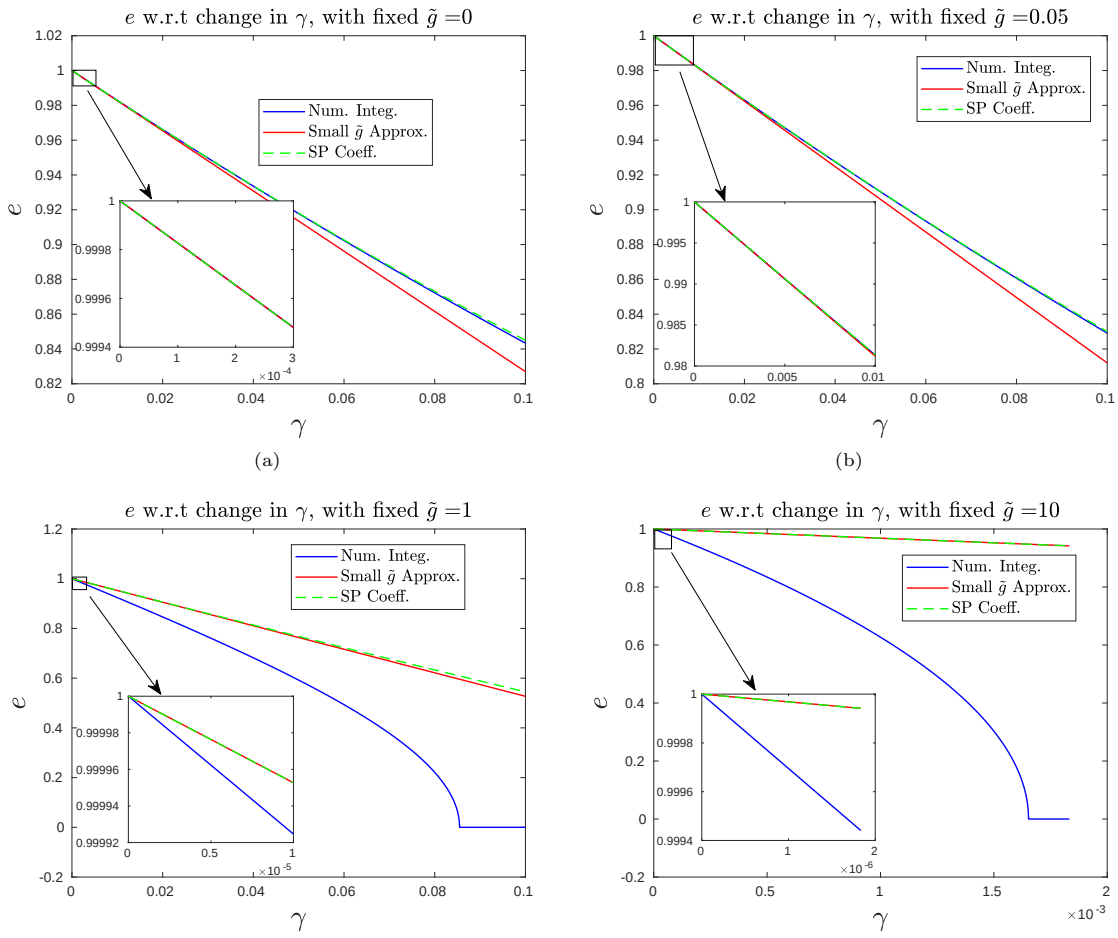

Fig. 7 For the Kuwabara-Kono model ($\alpha = \beta = 3/2$), comparison between the CoR values computed via numerical integration of (6) (plots labeled *Num. Integ.*), the $\mathcal{O}(\gamma)$ expansion (18) (plots labeled *Small* $\tilde{g}$ *Approx.*), and the $\mathcal{O}(\gamma^2)$ expansion (23) including the Schwager-Pöschel coefficient C_2 in (29) (plots labeled *SP Coeff.*), for $\gamma \in [0, 1]$ and (a) $\tilde{g} = 0$, (b) $\tilde{g} = 0.05$, (c) $\tilde{g} = 1$, (d) $\tilde{g} = 10$. Zoomed plots for $\gamma \approx 0$ are included in each panel.

substituting $\frac{\partial^2 u}{\partial \tau^2}$ from (30) :

$$\begin{aligned}\mathcal{I}(\gamma, \tilde{g}) &= -\frac{1}{\beta}\int_0^{T_f} \frac{\partial^2 u}{\partial \tau^2} u^\beta d\tau \\ &= \frac{1}{\beta}\int_0^{T_f} u^\beta (u^\alpha - \tilde{g}) d\tau,\end{aligned} \tag{33}$$

noting that $u(\gamma, 0) = u(\gamma, T_f) = 0$.

Differentiating $\mathcal{I}(\gamma, \tilde{g})$ with respect to γ, using the Leibniz integral rule and then substituting $u(\gamma, T_f) = 0$ leads to

$$\begin{aligned}\frac{\partial \mathcal{I}}{\partial \gamma}(\gamma, \tilde{g}) = \frac{1}{\beta}\int_0^{T_f} \frac{\partial u}{\partial \gamma} \big[(\beta+\alpha)u^{\beta+\alpha-1} \\ -\tilde{g}\beta u^{\beta-1}\big] d\tau.\end{aligned} \tag{34}$$

Thus, the expansion of (32) for $\gamma \approx 0$ can be expressed in terms of (33) and (34),

$$e^2 = 1 - 2\beta\mathcal{I}(0, \tilde{g})\gamma - 2\beta\frac{\partial \mathcal{I}}{\partial \gamma}(0, \tilde{g})\gamma^2 + \text{H.O.T.} \tag{35}$$

The coefficient $\mathcal{I}(0, \tilde{g}) = \mathcal{I}_0(\tilde{g})$ was previously introduced in (11) and expressed as the integral (12). In Appendix B, we compute $\frac{\partial \mathcal{I}}{\partial \gamma}(0, \tilde{g})$

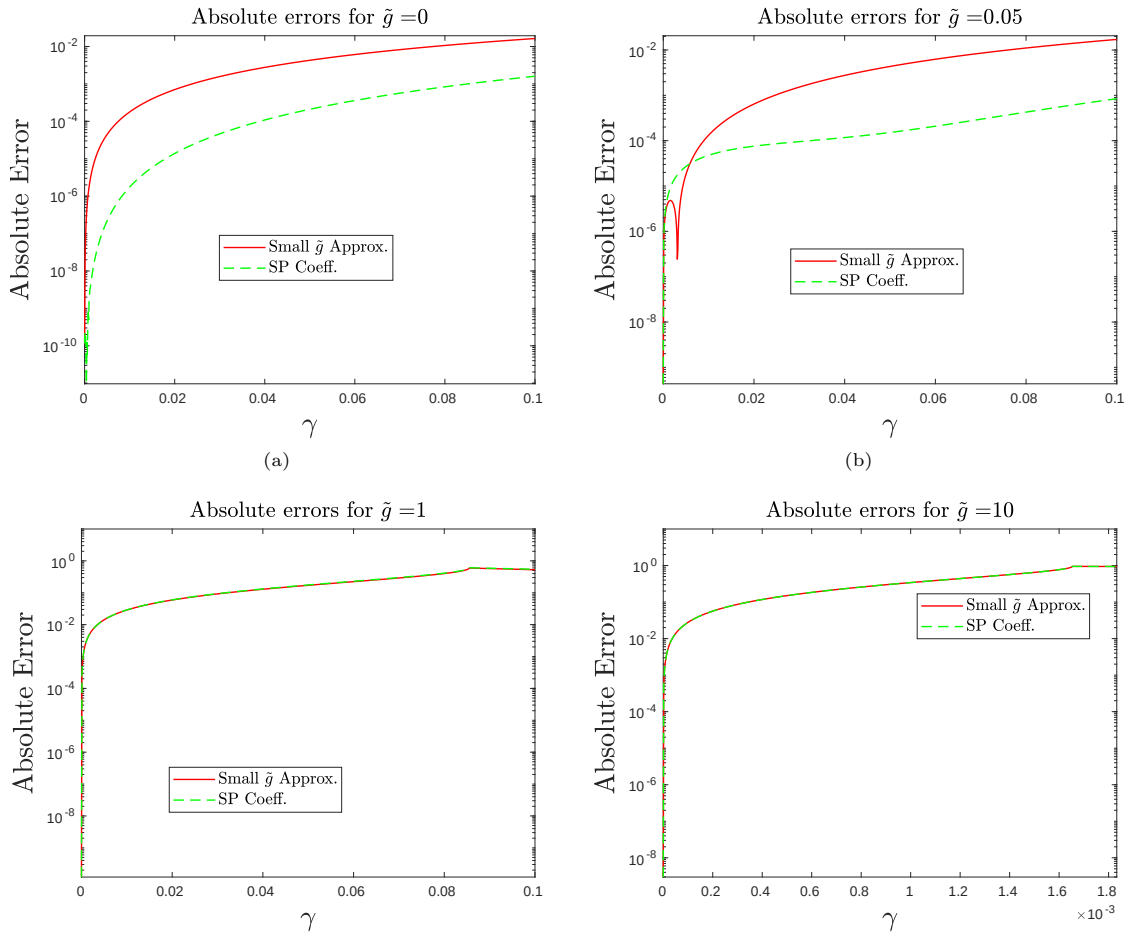

Fig. 8 For the Kuwabara-Kono model ($\alpha = \beta = 3/2$), absolute errors on the CoR e corresponding to the $\mathcal{O}(\gamma)$ expansion (18) (plots labeled *Small $\tilde{g}$ Approx.*) and the $\mathcal{O}(\gamma^2)$ expansion (23) (plots labeled *SP Coeff.*), for $\gamma \in [0, 1]$ and (a) $\tilde{g} = 0$, (b) $\tilde{g} = 0.05$, (c) $\tilde{g} = 1$, (d) $\tilde{g} = 10$. Errors are determined by comparison with direct numerical integration of (6).

(equations (B18) and (B20)) and deduce from (35) the following approximation of the CoR e:

Proposition 1 *A $\mathcal{O}(\gamma^2)$ approximation of the coefficient of restitution e is given by*

$$e \approx \min\left(e_+, e_s\right), \tag{36}$$

where

$$e_+ = \max\left(1 - 2\beta\mathcal{I}_0(\tilde{g})\gamma + 2\beta^2\mathcal{I}_0(\tilde{g})\mathcal{Q}_0(\tilde{g})\gamma^2, 0\right)^{1/2}, \tag{37}$$

$$e_s = \max\left(1 - \beta\mathcal{I}_0(\tilde{g})\gamma + \beta^2\mathcal{I}_0(\tilde{g})[\mathcal{Q}_0(\tilde{g}) - \frac{\mathcal{I}_0(\tilde{g})}{2}]\gamma^2, 0\right). \tag{38}$$

The functions $\mathcal{I}_0(\tilde{g})$ and $\mathcal{Q}_0(\tilde{g})$ are integrals given by

$$\mathcal{I}_0(\tilde{g}) = 2\int_0^{u_M}\left[1 + 2\left(\tilde{g}\,u_0 - \frac{u_0^{\alpha+1}}{\alpha+1}\right)\right]^{\frac{1}{2}} u_0^{\beta-1}du_0 \tag{39}$$

and

$$\mathcal{Q}_0(\tilde{g}) = \int_0^{u_M}\left[1 + 2\left(\tilde{g}\,u_0 - \frac{u_0^{\alpha+1}}{\alpha+1}\right)\right]^{-\frac{1}{2}} u_0^{\beta-1}du_0, \tag{40}$$

where the maximal compression u_M is solution of (13).

Proof. See Appendix B. □

Approximations (37) and (38) have the same second order Taylor expansion at $\gamma = 0$

$$e = 1 - A_1(\tilde{g})\,\gamma - A_2(\tilde{g})\,\gamma^2 + \text{H.O.T.}, \qquad (41)$$

with

$$A_1 = \beta \mathcal{I}_0, \quad A_2 = \beta^2 \mathcal{I}_0 \Big(\frac{\mathcal{I}_0}{2} - \mathcal{Q}_0\Big). \qquad (42)$$

In (36) we consider the minimum of the two approximations because we numerically observe that they tend to overestimate the CoR, and the best approximation depends on the parameter range (see [39]). Approximation (36) is theoretically valid for $\gamma \approx 0$ (since it follows from the perturbative expansion (35)), which corresponds to a standard parameter regime for the viscoelastic models (1). Our analysis does not provide an estimate of the maximal range of validity of (36), but for physical consistency the approximation must be used only in parameter ranges where (36) decreases with γ (which is the case when γ is small enough). In section 4.6, we will validate the CoR approximation by comparing (36) with a direct numerical integration of (6).

Now let us examine the result of Proposition 1 in the particular case $\tilde{g} = 0$. We have seen in section 4.2 that the integral $\mathcal{I}_0(0) = C_0/\beta$ can be computed using Euler's Beta function B and reads (see equation (20))

$$\mathcal{I}_0(0) = \left(\frac{\alpha+1}{2}\right)^{\frac{\beta}{\alpha+1}-1} \mathrm{B}\left(\frac{\beta}{\alpha+1}, \frac{3}{2}\right). \qquad (43)$$

Similarly, we find using (14) and (19)

$$\begin{aligned}\mathcal{Q}_0(0) &= \int_0^{\left(\frac{\alpha+1}{2}\right)^{\frac{1}{\alpha+1}}} u_0^{\beta-1}\left(1 - 2\frac{u_0^{\alpha+1}}{\alpha+1}\right)^{-\frac{1}{2}} du_0 \\ &= \frac{1}{2}\left(\frac{\alpha+1}{2}\right)^{\frac{\beta}{\alpha+1}-1} \mathrm{B}\left(\frac{\beta}{\alpha+1}, \frac{1}{2}\right).\end{aligned} \qquad (44)$$

Hence, if we substitute (43) and (44) into (41)-(42), we obtain for $\gamma \approx 0$

$$e_{|\tilde{g}=0} = 1 - \gamma C_0 - \gamma^2 C_2 + \text{H.O.T.},$$

with C_0 given in (20) and

$$C_2 = -\frac{\beta^3(\alpha+1)^{\frac{2\beta}{\alpha+1}-1}}{2^{\frac{2\beta}{\alpha+1}-2}(\alpha+2\beta+1)^2}\left[\mathrm{B}\left(\frac{\beta}{\alpha+1}, \frac{1}{2}\right)\right]^2. \qquad (45)$$

For $\alpha = \beta = \frac{3}{2}$, we have previously checked that $C_0 \approx 1.7302$ agrees with the value derived in [35]. Similarly, we obtain $C_2 \approx -1.7961$ in agreement with (29), hence the CoR expansion (41) agrees with the $\mathcal{O}(\gamma^2)$ expansion obtained in [35] for the Kuwabara-Kono model when $\tilde{g} = 0$.

As a corollary of Proposition 1 (considering the limit case $\tilde{g} \approx 0$), we obtain the CoR expansion (23) for arbitrary $\alpha, \beta \geq 1$. This result is summarized below.

Proposition 2 *Fix $\alpha, \beta \geq 1$. The second order Taylor expansion of the coefficient of restitution $e(\gamma, \tilde{g})$ at $(\gamma, \tilde{g}) = (0, 0)$ reads*

$$e = 1 - \gamma C_0 - \gamma\tilde{g} C_1 - \gamma^2 C_2 + \text{H.O.T.}, \qquad (46)$$

with coefficients C_i given in (20) and (45).

4.5 Approximate CoR in terms of Euler's Beta function

The $\mathcal{O}(\gamma^2)$ CoR approximation given in Proposition 1 involves integral functions $\mathcal{I}_0, Q_0$ depending on $\tilde{g}$ and defined in (39), (40). While these integrals can be expressed in terms of Euler's Beta function in the limits $\tilde{g} = 0$ and $\tilde{g} \to +\infty$, an explicit form is unknown for fixed $\tilde{g} \in (0, +\infty)$. In this section, we tackle this problem by constructing accurate approximations of (39), (40) as linear combinations of Beta functions for arbitrary $\tilde{g} \geq 0$.

Since the maximal compression u_M in the integrals (39) and (40) is an implicit function of $\tilde{g} \in [0, \infty)$ defined via equation (13), it is convenient to introduce the new parameter $\theta \in (0, 1]$ defined through

$$\frac{u_M^{\alpha+1}}{\alpha+1} = \frac{1}{2\theta}, \qquad (47)$$

so that (13) becomes

$$\tilde{g}(\theta) = \left(\frac{2\theta}{\alpha+1}\right)^{\frac{1}{\alpha+1}}\left(\frac{1}{2\theta} - \frac{1}{2}\right).$$

We have then

$$\theta = 1 \Leftrightarrow \tilde{g} = 0, \text{ and } \theta \to 0^+ \Leftrightarrow \tilde{g} \to +\infty. \qquad (48)$$

With the change of variable $u_0 = u_M x$ in the integrals $\mathcal{I}_0(\tilde{g}(\theta))$, $\mathcal{Q}_0(\tilde{g}(\theta))$, one obtains

$$\mathcal{I}_0\left(\tilde{g}(\theta)\right) = \frac{2}{\sqrt{\theta}}\left(\frac{\alpha+1}{2\theta}\right)^{\frac{\beta}{\alpha+1}} J_{\alpha,\beta}(\theta), \tag{49}$$

$$\mathcal{Q}_0\left(\tilde{g}(\theta)\right) = \sqrt{\theta}\left(\frac{\alpha+1}{2\theta}\right)^{\frac{\beta}{\alpha+1}} M_{\alpha,\beta}(\theta), \tag{50}$$

with

$$\begin{aligned} J_{\alpha,\beta}(\theta) &= \int_0^1 \left[\theta + (1-\theta)x - x^{\alpha+1}\right]^{\frac{1}{2}} x^{\beta-1} dx, \\ M_{\alpha,\beta}(\theta) &= \int_0^1 \left[\theta + (1-\theta)x - x^{\alpha+1}\right]^{-\frac{1}{2}} x^{\beta-1} dx, \end{aligned} \tag{51}$$

where we have used (47) and the identities

$$u_M = \left(\frac{\alpha+1}{2\theta}\right)^{\frac{1}{\alpha+1}}, \quad \tilde{g}\, u_M = \frac{1-\theta}{2\theta}.$$

The integrals $J_{\alpha,\beta}(\theta)$ and $M_{\alpha,\beta}(\theta)$ can be expressed in terms of Euler's Beta function when $\theta = 0$ and $\theta = 1$, but do not have a similar exact representation when $\theta \in (0,1)$. However, we will be able to approximate these integrals as linear combinations of Beta functions.

We first note that the two families of integrals $J_{\alpha,\beta}(\theta)$ and $M_{\alpha,\beta}(\theta)$ are related, therefore we only need to approximate $M_{\alpha,\beta}(\theta)$ and use the resulting approximation to obtain $J_{\alpha,\beta}(\theta)$. Indeed, using the identity

$$\begin{aligned} &\tfrac{\alpha+1}{2\beta} M_{\alpha,\alpha+\beta+1}(\theta) + \tfrac{\theta-1}{2\beta} M_{\alpha,\beta+1}(\theta) \\ &= \tfrac{-1}{2\beta} \int_0^1 x^\beta \left[1 - \theta - (\alpha+1)x^\alpha\right] \\ &\qquad \times \left[\theta + (1-\theta)x - x^{\alpha+1}\right]^{-\frac{1}{2}} dx \end{aligned}$$

and then integrating by parts, one finds

$$J_{\alpha,\beta}(\theta) = \frac{\alpha+1}{2\beta} M_{\alpha,\alpha+\beta+1}(\theta) + \frac{\theta-1}{2\beta} M_{\alpha,\beta+1}(\theta). \tag{52}$$

The approximation of $M_{\alpha,\beta}(\theta)$ is described in the following Proposition.

Proposition 3 *Let n be an odd integer. An approximation of the integral $M_{\alpha,\beta}(\theta)$ is given by the following quadrature formula based on Chebyshev interpolation :*

$$M_{\alpha,\beta}(\theta) \simeq \frac{c_0}{2}\, a_{0,0} + \sum_{2 \le j \le n-1,\ j \text{ even}} c_j\, a_{j,0}, \tag{53}$$

where the terms $a_{j,k}$ involve Euler's Beta function B *and are defined by induction as follows:*

$$\begin{cases} a_{j+2,k} = 2a_{j+1,k+1} - 2a_{j+1,k} - a_{j,k} \text{ for } j \ge 0, \\ \text{with} \quad a_{0,k} = \frac{1}{\alpha+\theta}\, \mathrm{B}\left(\frac{\beta+k-1/2+\theta/2}{\alpha+\theta}, \frac{1}{2}\right), \\ \text{and} \quad a_{1,k} = a_{0,k+1} - a_{0,k}. \end{cases} \tag{54}$$

The coefficients c_j ($j \ge 0$ and even) are defined by

$$c_j = \frac{4}{n+1} \sum_{k=(n+1)/2}^{n} h_{\alpha,\theta}(x_k) \cos\left(j\pi \frac{2k+1}{2n+2}\right), \tag{55}$$

where

$$h_{\alpha,\theta}(x) = \left(\frac{x^{1-\theta} - x^{\alpha+1}}{\theta + (1-\theta)x - x^{\alpha+1}}\right)^{\frac{1}{2}}, \tag{56}$$

and x_k are Chebyshev nodes in the range $[0,2]$

$$x_k = \cos\left(\pi \frac{2k+1}{2n+2}\right) + 1, \quad 0 \le k \le n. \tag{57}$$

Proof. See Appendix C. □

The idea of Proposition 3 is to replace the integrand $(x^{1-\theta} - x^{\alpha+1})^{-1/2} x^{\beta-1}\, h_{\alpha,\theta}(x)$ in (51) by a function of the form $(x^{1-\theta} - x^{\alpha+1})^{-1/2} x^{\beta-1} P(x)$ for some polynomial P approximating $h_{\alpha,\theta}$, leading to an integral that can be expressed as a sum of Beta functions. The polynomial P is constructed by interpolating $h_{\alpha,\theta}$ at Chebyshev nodes. The special cases $\theta = 0$ and $\theta = 1$ (corresponding respectively to the limits of infinite and vanishing $\tilde{g}$) lead to $h_{\alpha,\theta} = 1 = P$, hence the approximation becomes exact in these limiting cases. The evaluation of the approximation (53) of $M_{\alpha,\beta}(\theta)$ requires computation of the terms $a_{j,k}$ using the recurrence relations in (54), following the scheme described in Table 1.

The integer n corresponds to the degree of the polynomial interpolation and must be carefully selected. It must be large enough to obtain a precise approximation of the integral $M_{\alpha,\beta}(\theta)$, but small enough to avoid numerical instabilities. In [39], the validity of the approximation of $M_{\alpha,\beta}(\theta)$ is studied by comparison with numerical integral

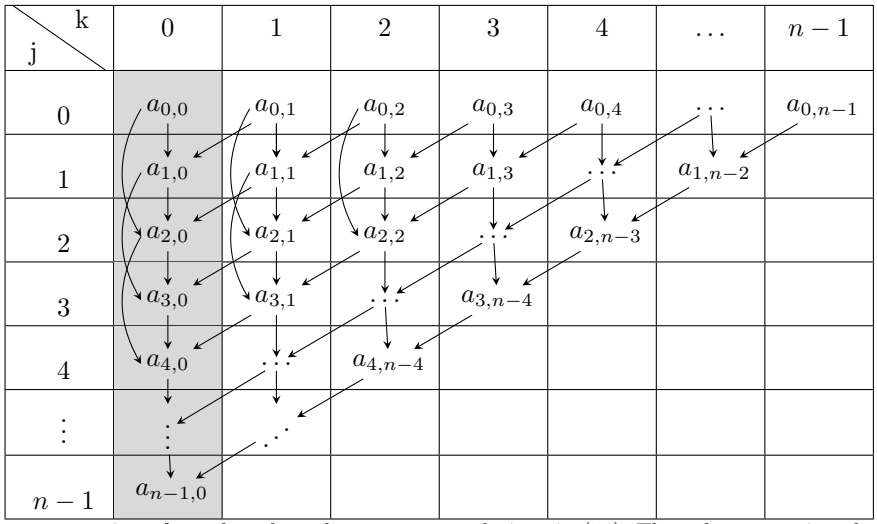

Table 1 Tabular computation of $a_{j,k}$ based on the recurrence relations in (54). The values $a_{2p,0}$ in column $k = 0$ (highlighted in gray) are required for the final computation of $M_{\alpha,\beta}(\theta)$.

computations. It is found that an order $n = 21$ works best and leads to accurate approximations. For example, for $\alpha = \beta = 3/2$ (Kuwabara-Kono model) the maximum relative error on $M_{\alpha,\beta}(\theta)$ is in the order of 10^{-4}. This allow us to accurately approximate the integral $J_{\alpha,\beta}$ in (52) and the integrals $\mathcal{I}_0$, $\mathcal{Q}_0$ with (49), (50), leading to a precise approximation of the different terms in the CoR expansion (36). Consequently we shall fix $n = 21$ in the numerical results presented henceforth.

4.6 Numerical results

In this section we study numerically the validity of the $\mathcal{O}(\gamma^2)$ approximation of the CoR e given in Proposition 1. We fix $\alpha = 3/2$ (Hertz contact case) and consider three types of dissipation : linear damping $\beta = 1$ (Fig. 9), Kuwabara-Kono model $\beta = 3/2$ (Fig. 10) and Simon-Hunt-Crossley model $\beta = 5/2$ (Fig. 11). Additional results for the Tsuji-Tanaka-Ishida model $\beta = 5/4$ and the linear spring-dashpot model $\alpha = \beta = 1$ are available in the supplementary technical report [39].

For each model, we plot the CoR e versus the rescaled dissipation constant $\gamma \in [0, 0.1]$. This is done for different values of the rescaled external load $\tilde{g}$, either vanishing, small, intermediate or large ($\tilde{g} = 0$, 0.05, 1, and 10). These graphs are completed by Tables 2, 3 and 4, where we indicate for each value of β the maximal absolute error of approximation on e within certain ranges of γ (error graphs can be found in [39]). The range $\gamma \leq 0.1$ in (3) is appropriate for low velocity impacts involving various types of materials, see Fig. 2 for an example and [27, 40, 41] for estimates of γ in the Kuwabara-Kono model. Similarly, assuming $\tilde{g} \leq 10$ in (4) accounts for a valuable range of external loads for low velocity impacts.

One can observe that the $\mathcal{O}(\gamma^2)$ approximation (36) remains essentially unchanged if its integral coefficients $\mathcal{I}_0(\tilde{g})$, $\mathcal{Q}_0(\tilde{g})$ given by (39), (40) are directly numerically computed (graphs labeled *Num. Coeffs.*) or approximated by sums of Beta functions following the method of section 4.5 (graphs labeled *Approx. Coeffs.*). Indeed, the graphs corresponding to the two versions of the $\mathcal{O}(\gamma^2)$ approximation almost coincide in Figs. 9–11. The direct numerical integration of $\mathcal{I}_0(\tilde{g})$, $\mathcal{Q}_0(\tilde{g})$ for $\tilde{g} > 0$ is performed using the `ode45` solver of `MATLAB` (with absolute and relative error tolerances set to 10^{-8} and 10^{-7}), using root finding option (event detection) to compute the upper bound $u_M(\tilde{g})$ [44]. Also, we recall that $\mathcal{I}_0(0)$, $\mathcal{Q}_0(0)$ can be calculated via Euler's Beta function by formulas (43), (44) (graphs labeled *Exact Coeffs.*) and that their approximations in Section 4.5 become exact for $\tilde{g} = 0$ and $\tilde{g} \to +\infty$.

In addition, the accuracy of the analytical approximations of e is determined by comparing

them to the CoR obtained by numerical time integration of (6) (graphs labeled *Num. Integ.*). From Fig. 10 for $\beta = 3/2$, one can see that the local approximation (46) (second order Taylor expansion of e at $(\gamma, \tilde{g}) = (0, 0)$) is precise if $\tilde{g}$ is small (Fig. 10(a)-(b), graphs labeled *SP Coeff.*), and its accuracy is essentially equivalent to that of approximation (36) in Proposition 1 (for γ not too small [39]). However, approximation (46) breaks down for moderate or large $\tilde{g}$, while approximation (36) remains valid in such parameter regimes (Fig. 10(c)-(d)).

More precisely, our computations show that for $\gamma \in [0, 0.1]$, the CoR approximation in Proposition 1 is very accurate when $\tilde{g}$ is either small or large (Fig. 9–11, panels (a)-(b)-(d)). In particular, when $\tilde{g}$ is large the critical dissipation $\gamma_c \ll 1$ above which $e = 0$ is very well approximated in panels (d). For intermediate values of $\tilde{g}$, the CoR approximation is not accurate for $\gamma \approx \gamma_c$ due to the fast cancellation of the numerical CoR (Fig. 10(c) and 11(c)), and we notice that the error increases with the dissipation exponent β. However, the approximation remains very precise when $\gamma \ll \gamma_c$ (see the insets in panels (c)). More quantitative information is given in error Tables 2–4. A general conclusion is that the analytical CoR formula (36) from Proposition 1 and section 4.5 accurately approximates the exact CoR of model (2) for a valuable range of parameters γ and $\tilde{g}$.

5 Recapitulation

This section presents a brief summary of the method for computing the analytical CoR approximation of Proposition 1, for a single spherical bead undergoing impact in the presence of a constant external load. The fundamental set of quantities needed for this computation is given by:

m : mass of the bead,
k : stiffness constant in the nonlinear viscoelastic contact model (1),
α : exponent in the contact force versus displacement (deformation) in model (1) ($\alpha = 3/2$ for Hertz contact),
β : exponent on the nonlinear dissipative term in model (1),
γ_0 : dissipation constant in model (1),
F : constant external load on the bead,
g : gravitational acceleration constant,
v_0 : impact velocity of the bead.

The first step is to combine the aforementioned parameters into the two dimensionless parameters

$$\gamma = \gamma_0 v_0^{\frac{2\beta}{\alpha+1}-1} \left(\frac{k}{m}\right)^{1-\frac{\beta}{\alpha+1}}$$

$$\text{and } \tilde{g} = \left(\frac{m}{k}\right)^{\frac{1}{\alpha+1}} v_0^{\frac{-2\alpha}{\alpha+1}} \left(g + \frac{F}{m}\right).$$

Then one computes the integrals $\mathcal{I}_0(\tilde{g})$ and $\mathcal{Q}_0(\tilde{g})$ defined in (39) and (40), involved in the $\mathcal{O}(\gamma^2)$ approximation (36). These integrals can be either calculated numerically or analytically approximated. The steps for computing the analytical approximations of $\mathcal{I}_0(\tilde{g})$ and $\mathcal{Q}_0(\tilde{g})$ are listed below:

1 Solve for $\theta \in (0, 1]$, such that $\tilde{g} = \left(\frac{2\theta}{\alpha+1}\right)^{\frac{1}{\alpha+1}} \frac{1-\theta}{2\theta}$ (e.g. using the bisection method or Newton's method).
2 Next to approximate the integral $M_{\alpha,\beta}(\theta)$ defined in (51), first choose a degree of interpolation n (ideally $n = 21$) and use the analytical approximation (53) defined in Proposition 3 through formulas (54) and (55). The coefficients $a_{j,0}$ in (53) are obtained using the computation scheme described in Table 1.
3 Following the same procedure as in the previous step, compute $M_{\alpha,\alpha+\beta+1}(\theta)$ and $M_{\alpha,\beta+1}(\theta)$. Then use these values to compute $J_{\alpha,\beta}(\theta)$ according to (52).
4 Compute $\mathcal{I}_0 = \frac{2}{\sqrt{\theta}}\left(\frac{\alpha+1}{2\theta}\right)^{\frac{\beta}{\alpha+1}} J_{\alpha,\beta}(\theta)$ and $\mathcal{Q}_0 = \sqrt{\theta}\left(\frac{\alpha+1}{2\theta}\right)^{\frac{\beta}{\alpha+1}} M_{\alpha,\beta}(\theta)$.

Lastly, calculate the analytical approximation (36) of the CoR e using the values of $\mathcal{I}_0$, $\mathcal{Q}_0$ and γ. The `MATLAB` implementation of the aforementioned method is available at [44] along with all numerical results presented in this article.

6 Conclusion

The goal of this study was to derive an approximate analytical expression of the coefficient of restitution (CoR) for a single bead impact, while considering the effects of a constant external force. We derived several expansions of the CoR based on a general nonlinear viscoelastic model and studied their accuracy with respect to calculations of CoR from numerical time integration. We

Types of $\mathcal{I}_0$ & $\mathcal{Q}_0$	Exact[(43),(44)]/Num.[(39),(40)]		Approx.[(52),(53)]	
$\tilde{g}$	$\gamma < 0.02$	$\gamma \geq 0.02$	$\gamma < 0.02$	$\gamma \geq 0.02$
0	5.39×10^{-6}*	6.57×10^{-4}*	5.39×10^{-6}	6.57×10^{-4}
0.05	5.63×10^{-6}	6.89×10^{-4}	1.32×10^{-5}	7.26×10^{-4}
1	6.82×10^{-5}	1.77×10^{-2}	1.32×10^{-4}	1.85×10^{-2}

(a) Max. absolute errors within different γ ranges for $\tilde{g} = 0, 0.05,$ and, 1

Type of $\mathcal{I}_0$ & $\mathcal{Q}_0$	$\gamma < 0.0011$	$0.0011 \leq \gamma \leq 0.0051$	$\gamma > 0.0051$
Num.[(39),(40)]	4.39×10^{-7}	4.25×10^{-3}	5.63×10^{-13}
Approx.[(52),(53)]	8.03×10^{-5}	1.33×10^{-2}	5.63×10^{-13}

(b) Max. absolute errors within different γ ranges for $\tilde{g} = 10$

Table 2 Maximum absolute errors on the CoR e from the analytical approximation (36) in various γ ranges, for $\alpha = 3/2$ and $\beta = 1$ (Hertz stiffness with linear damping) and (a) $\tilde{g} = 0$, 0.05, 1, (b) $\tilde{g} = 10$. Integral coefficients (39), (40) in (36) are either approximated via formulas (52)-(53) or numerically computed, using the exact formulas (43), (44) in the special case $\tilde{g} = 0$ (*).

Types of $\mathcal{I}_0$ & $\mathcal{Q}_0$	Exact[(43),(44)]/Num.[(39),(40)]		Approx.[(52),(53)]	
$\tilde{g}$	$\gamma < 0.02$	$\gamma \geq 0.02$	$\gamma < 0.02$	$\gamma \geq 0.02$
0	1.37×10^{-5}*	1.60×10^{-3}*	1.37×10^{-5}	1.60×10^{-3}
0.05	1.52×10^{-5}	1.78×10^{-3}	2.33×10^{-5}	1.82×10^{-3}
1	3.67×10^{-4}	2.08×10^{-1}	4.58×10^{-4}	2.09×10^{-1}

(a) Max. absolute errors within different γ ranges for $\tilde{g} = 0, 0.05,$ and, 1

Types of $\mathcal{I}_0$ & $\mathcal{Q}_0$	$\gamma < 0.000367$	$0.000367 \leq \gamma \leq 0.00169$	$\gamma > 0.00169$
Num.[(39),(40)]	1.06×10^{-7}	2.38×10^{-4}	2.84×10^{-13}
Approx.[(52),(53)]	8.11×10^{-5}	2.11×10^{-2}	2.84×10^{-13}

(b) Max. absolute errors within different γ for $\tilde{g} = 10$

Table 3 Maximum absolute errors on the CoR e from the analytical approximation (36) in various γ ranges, for $\alpha = \beta = 3/2$ (Kuwabara-Kono model) and (a) $\tilde{g} = 0$, 0.05, 1, (b) $\tilde{g} = 10$. Integral coefficients (39), (40) in (36) are either approximated via formulas (52)-(53) or numerically computed, using the exact formulas (43), (44) in the special case $\tilde{g} = 0$ (*).

Types of $\mathcal{I}_0$ & $\mathcal{Q}_0$	Exact[(43),(44)]/Num.[(39),(40)]		Approx.[(52),(53)]	
$\tilde{g}$	$\gamma < 0.02$	$\gamma \geq 0.02$	$\gamma < 0.02$	$\gamma \geq 0.02$
0	3.87×10^{-5}*	4.26×10^{-3}*	3.87×10^{-5}	4.26×10^{-3}
0.05	4.94×10^{-5}	5.39×10^{-3}	5.84×10^{-5}	5.43×10^{-3}
1	2.06×10^{-3}	3.11×10^{-1}	2.20×10^{-3}	3.11×10^{-1}

(a) Max. absolute errors within different γ ranges for $\tilde{g} = 0, 0.05,$ and, 1

Types of $\mathcal{I}_0$ & $\mathcal{Q}_0$	$\gamma < 0.00004$	$0.00004 \leq \gamma \leq 0.00020$	$\gamma > 0.00020$
Num.[(39),(40)]	3.83×10^{-7}	9.67×10^{-4}	2.84×10^{-13}
Approx.[(52),(53)]	8.57×10^{-5}	2.50×10^{-1}	2.84×10^{-13}

(b) Max. absolute errors within different γ for $\tilde{g} = 10$

Table 4 Maximum absolute errors on the CoR e from the analytical approximation (36) in various γ ranges, for $\alpha = 3/2$ and $\beta = 5/2$ (Simon-Hunt-Crossley model) and (a) $\tilde{g} = 0$, 0.05, 1, (b) $\tilde{g} = 10$. Integral coefficients (39), (40) in (36) are either approximated via formulas (52)-(53) or numerically computed, using the exact formulas (43), (44) in the special case $\tilde{g} = 0$ (*).

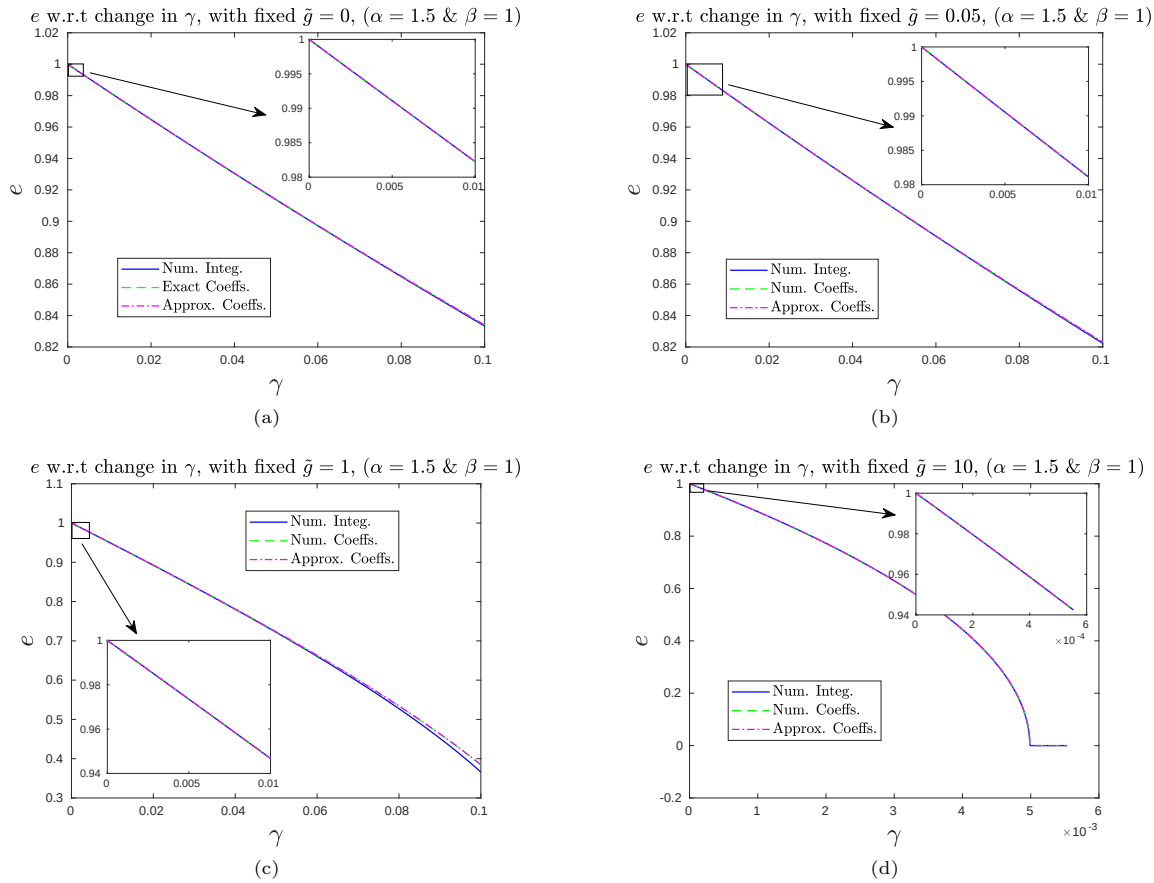

Fig. 9 Comparison between the CoR computed via numerical time integration of (6) (label *Num. Integ.*) and the $\mathcal{O}(\gamma^2)$ approximations given by (36), using the numerically computed integrals $\mathcal{I}_0$ and $\mathcal{Q}_0$ from (39) and (40) (label *Num. Coeffs.*) and the approximated integrals (49)-(50)-(52)-(53) (label *Approx. Coeffs.*). When $\tilde{g} = 0$, $\mathcal{I}_0$ and $\mathcal{Q}_0$ are calculated using (43) and (44) (label *Exact Coeffs.*). Results are shown for the viscoelastic model with $\alpha = 3/2$ and $\beta = 1$ (Hertz stiffness with linear damping), for the cases: (a) $\tilde{g} = 0$, (b) $\tilde{g} = 0.05$, (c) $\tilde{g} = 1$, and (d) $\tilde{g} = 10$.

obtained first-order expansions with respect to the small dimensionless parameter γ corresponding to a rescaled dissipation constant, both for small and large magnitudes of the rescaled external force $\tilde{g}$. This allowed us to derive a critical external force $\tilde{g}_c(\gamma)$ (or equivalently a critical damping $\gamma_c(\tilde{g})$) cancelling the CoR, and above which the bead does not rebound. In order to approximate the CoR over a larger range of γ values, we derived a correction to the above approximation including a quadratic term in γ. We computed the quadratic coefficient for a general viscoelastic model, thereby generalizing a result of [32, 35] valid for the Kuwabara-Kono model and in the absence of gravity. This second-order CoR expansion improved the approximation for small $\tilde{g}$, but didn't perform well for higher values (i.e. when the external force is large, or is finite with a small impact velocity). Hence, we derived an improved second-order expansion of the CoR with respect to γ, with coefficients given by integrals depending on a rescaled external force $\tilde{g}$ of arbitrary magnitude. Performing a numerical computation of the integral coefficients, we observed that this approximation of the CoR is very accurate for most parameter values. We further improved this result by providing an approximation of the integral coefficients in terms of Euler's Beta function, while preserving the overall precision of the expansion of the CoR.

An interesting extension to this work would be to generalize the ($\tilde{g}$-dependent) second-order expansion in γ from Proposition 1 to higher orders. For the Kuwabara-Kono model in the

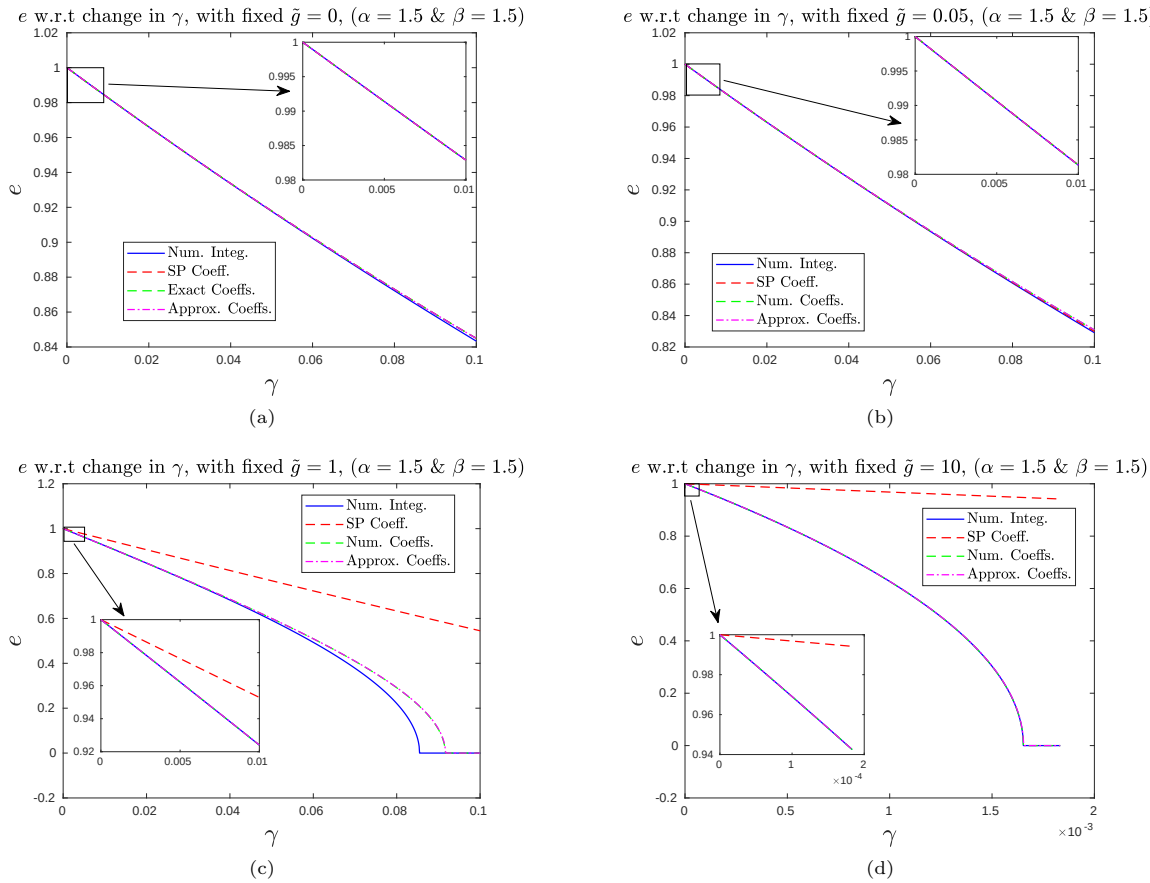

Fig. 10 Comparison between the CoR computed via numerical time integration of (6) (label *Num. Integ.*) and the $\mathcal{O}(\gamma^2)$ approximations given by (36), using the numerically computed integrals $\mathcal{I}_0$ and $\mathcal{Q}_0$ from (39) and (40) (label *Num. Coeffs.*) and the approximated integrals (49)-(50)-(52)-(53) (label *Approx. Coeffs.*). When $\tilde{g} = 0$, $\mathcal{I}_0$ and $\mathcal{Q}_0$ are calculated using (43) and (44) (label *Exact Coeffs.*). Results are shown for the viscoelastic model with $\alpha = \beta = 3/2$ (Kuwabara-Kono model), for the cases: (a) $\tilde{g} = 0$, (b) $\tilde{g} = 0.05$, (c) $\tilde{g} = 1$, and (d) $\tilde{g} = 10$. The second order Taylor approximation (46) at $(\gamma, \tilde{g}) = (0, 0)$ (with γ^2 coefficient taken from [35]) is also included for comparison (label *SP Coeff.*).

absence of gravity, this problem was addressed in [35] where an algorithm was provided to compute CoR expansions at arbitrary orders by induction. Such higher order expansions may be used (in conjunction with Padé approximants [33, 34]) to improve the CoR approximation when γ approaches the critical value γ_c from below, especially for intermediate values of $\tilde{g}$. Note that in this problem, complications can be expected for fractional powers α, β due to the limited smoothness of the right side of (6) at $u = 0^+$. In addition, as in [35] when $\beta < \alpha + 1$, one could derive similar CoR approximations when the end of collision is defined by a vanishing repulsive contact force (i.e., $u^{\alpha+1-\beta} + \beta\gamma\, u' = 0$ at $\tau = T_f$) instead of a vanishing bead deformation $u(T_f) = 0$.

Appendix A $\mathcal{O}(\gamma)$ expansion of the squared CoR and large $\tilde{g}$ limit

In this appendix we examine the $\mathcal{O}(\gamma)$ expansion (10) of the squared CoR obtained for $\gamma \ll 1$:

$$e^2 = 1 - 2\gamma\beta\mathcal{I}_0(\tilde{g}) + \text{H.O.T.}, \qquad \text{(A1)}$$

where

$$\mathcal{I}_0(\tilde{g}) = \int_0^{T_0} \left(\frac{du_0}{d\tau}\right)^2 u_0^{\beta-1} d\tau \qquad \text{(A2)}$$

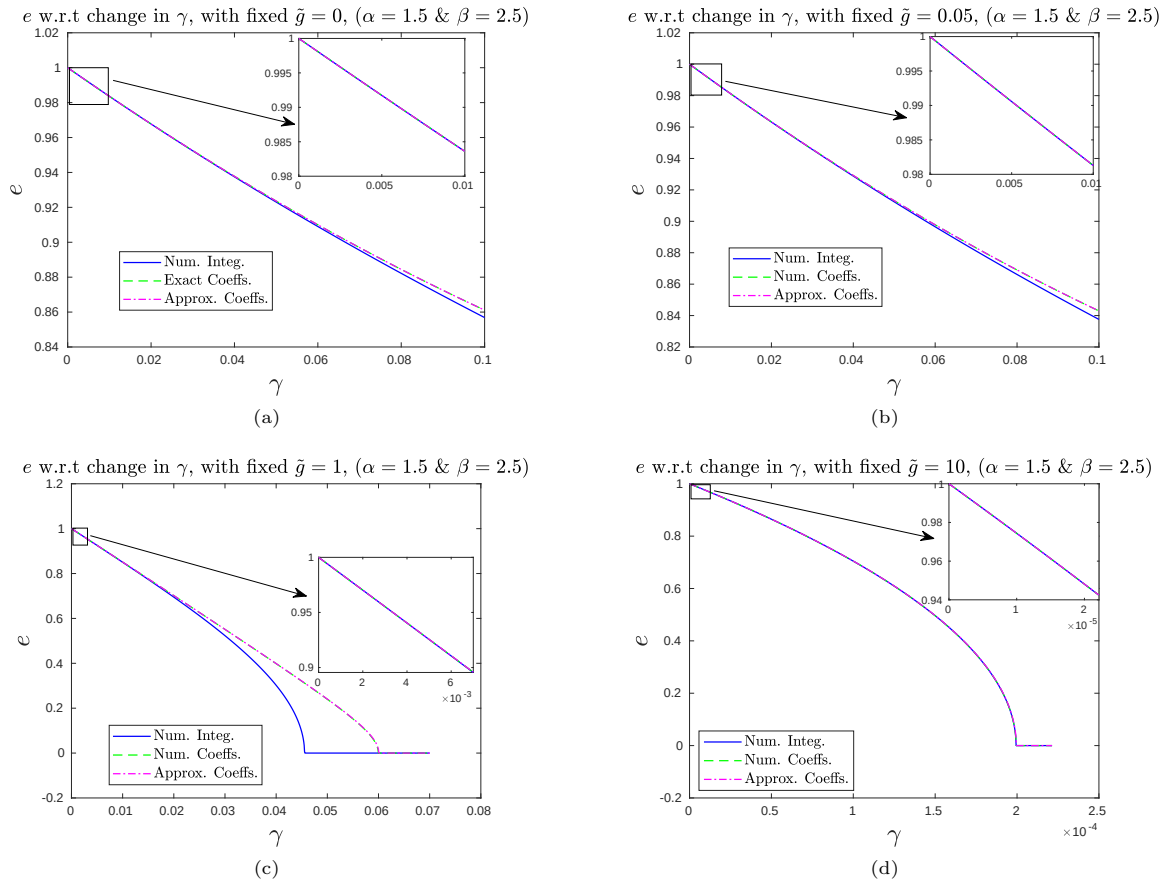

Fig. 11 Comparison between the CoR computed via numerical time integration of (6) (label *Num. Integ.*) and the $\mathcal{O}(\gamma^2)$ approximations given by (36), using the numerically computed integrals $\mathcal{I}_0$ and $\mathcal{Q}_0$ from (39) and (40) (label *Num. Coeffs.*) and the approximated integrals (49)-(50)-(52)-(53) (label *Approx. Coeffs.*). When $\tilde{g} = 0$, $\mathcal{I}_0$ and $\mathcal{Q}_0$ are calculated using (43) and (44) (label *Exact Coeffs.*). Results are shown for the viscoelastic model with $\alpha = 3/2$ and $\beta = 5/2$ (Simon-Hunt-Crossley model), for the cases: (a) $\tilde{g} = 0$, (b) $\tilde{g} = 0.05$, (c) $\tilde{g} = 1$, and (d) $\tilde{g} = 10$.

and $T_0 > 0$ corresponds to the end of impact in the absence of dissipation ($u_0(T_0) = 0$, $\frac{du_0}{d\tau}(T_0) = -1$). We shall simplify the integral coefficient (A2) for arbitrary $\tilde{g}$ and investigate the large $\tilde{g}$ limit.

Due to the symmetry $u_0\left(\frac{T_0}{2} + \tau\right) = u_0\left(\frac{T_0}{2} - \tau\right)$ about the maximal compression in the nondissipative case, we can rewrite the integral in (A2) as

$$\mathcal{I}_0(\tilde{g}) = 2\int_0^{\frac{T_0}{2}} \left(\frac{du_0}{d\tau}\right)^2 u_0^{\beta-1} d\tau. \tag{A3}$$

Multiplying (9) by $\frac{du_0}{d\tau}$ and integrating from $\tau = 0$ yields the energy conservation equation

$$\frac{1}{2}\left[\left(\frac{du_0}{d\tau}\right)^2 - 1\right] + \frac{{u_0}^{\alpha+1}}{\alpha+1} = \tilde{g}u_0,$$

which can be used to solve for $\frac{du_0}{d\tau}$ in the compression phase,

$$\frac{du_0}{d\tau} = \left[1 + 2\left(\tilde{g}u_0 - \frac{{u_0}^{\alpha+1}}{\alpha+1}\right)\right]^{\frac{1}{2}}. \tag{A4}$$

At the maximum compression one has $\frac{du_0}{d\tau}(T_0/2) = 0$, therefore the maximal deformation

$u_M = u_0(T_0/2)$ satisfies

$$\frac{1}{\alpha+1}{u_M}^{\alpha+1} = \tilde{g}u_M + \frac{1}{2}. \tag{A5}$$

Considering the integral in (A3) and changing integration variable ($\tau \to u_0$), we get using (A4)

$$\mathcal{I}_0(\tilde{g}) = 2\int_0^{u_M} \left[1 + 2\left(\tilde{g}u_0 - \frac{{u_0}^{\alpha+1}}{\alpha+1}\right)\right]^{\frac{1}{2}} {u_0}^{\beta-1} du_0. \tag{A6}$$

Let us now investigate the large $\tilde{g}$ limit. Equation (A5) yields

$$\frac{1}{\alpha+1}{u_M}^{\alpha+1} \approx \tilde{g}u_M$$

which suggests to introduce the new unknown y defined by

$$u_M = \tilde{g}^{\frac{1}{\alpha}} y. \tag{A7}$$

Substituting u_M from (A7) back into (A5), we obtain

$$\frac{1}{\alpha+1}y^{\alpha+1} - y = \frac{\epsilon}{2}, \tag{A8}$$

where $\epsilon = \frac{1}{\tilde{g}^{1+\frac{1}{\alpha}}}$ is a small parameter when $\tilde{g} \gg 1$. This yields

$$y = (1+\alpha)^{\frac{1}{\alpha}} + \mathcal{O}(\epsilon),$$

$$u_M = [\tilde{g}(1+\alpha)]^{\frac{1}{\alpha}} + \mathcal{O}\left(\frac{1}{\tilde{g}}\right).$$

In order to study the behavior of integral (A6) for $\tilde{g} \gg 1$, we perform the change of variable $u_0 = \tilde{g}^{\frac{1}{\alpha}} y_0$, which leads to

$$\mathcal{I}_0(\tilde{g}) = 2\tilde{g}^{\frac{\beta}{\alpha}+\frac{1}{2\alpha}+\frac{1}{2}} \times \int_0^{y} \left[\epsilon + 2\left(y_0 - \frac{{y_0}^{\alpha+1}}{\alpha+1}\right)\right]^{\frac{1}{2}} {y_0}^{\beta-1} dy_0. \tag{A9}$$

When $\epsilon \approx 0$, the integral (A9) can be approximated as

$$\mathcal{I}_0(\tilde{g}) = 2\sqrt{2}\tilde{g}^{\frac{\beta}{\alpha}+\frac{1}{2\alpha}+\frac{1}{2}} \times \int_0^{(1+\alpha)^{\frac{1}{\alpha}}} \left(1 - \frac{y_0^{\alpha}}{\alpha+1}\right)^{\frac{1}{2}} {y_0}^{\beta-\frac{1}{2}} dy_0 + \text{H.O.T.} \tag{A10}$$

Now we can consider another change of variable $t = \frac{{y_0}^{\alpha}}{\alpha+1}$, which yields using (19)

$$\mathcal{I}_0(\tilde{g}) = \frac{2\sqrt{2}}{\alpha}(\alpha+1)^{\frac{\beta+1/2}{\alpha}} \tilde{g}^{\frac{2\beta+\alpha+1}{2\alpha}} \mathrm{B}\left(\frac{\beta+\frac{1}{2}}{\alpha}, \frac{3}{2}\right). \tag{A11}$$

Thus, substituting (A11) into (A1) yields the large $\tilde{g}$ limit of the CoR expansion

$$e^2 \approx 1 - 2\gamma C \tilde{g}^{\left(\frac{\beta}{\alpha}+\frac{1}{2\alpha}+\frac{1}{2}\right)}, \tag{A12}$$

where

$$C = 2\sqrt{2}\frac{\beta}{\alpha}(\alpha+1)^{\left(\frac{\beta}{\alpha}+\frac{1}{2\alpha}\right)} \mathrm{B}\left(\frac{\beta+\frac{1}{2}}{\alpha}, \frac{3}{2}\right).$$

Appendix B Proof of Proposition 1

In this appendix we establish the $\mathcal{O}(\gamma^2)$ approximation of the CoR e stated in Proposition 1.

We start from the expansion (35) of e^2, where the integral $\frac{\partial \mathcal{I}}{\partial \gamma}(\gamma, \tilde{g})$ given in (34) needs to be computed at $\gamma = 0$. This step quite technical, therefore we shall summarize the main steps of the computation and refer to the technical report [39] for details.

Let us denote by u_0 the solution of (30)-(31) in the non-dissipative case $\gamma = 0$ and consider the corresponding impact duration T_0. In (35), we need to evaluate $\frac{\partial \mathcal{I}}{\partial \gamma}$ for $\gamma = 0$, so using (34) we can write

$$\frac{\partial \mathcal{I}}{\partial \gamma}(0, \tilde{g}) = \frac{1}{\beta}\int_0^{T_0} u_\gamma^0 \left[(\beta+\alpha){u_0}^{\beta+\alpha-1} - \tilde{g}\beta {u_0}^{\beta-1}\right] d\tau, \tag{B13}$$

where we note $u_\gamma^0(\tau) = \frac{\partial u}{\partial \gamma}(0, \tau)$. We need to compute u_γ^0 to further evaluate (B13). Differentiating (30)-(31) with respect to γ at $\gamma = 0$, we obtain the linear non-homogeneous problem

$$\frac{d^2 u_\gamma^0}{d\tau^2} + \alpha {u_0}^{\alpha-1} u_\gamma^0 + \frac{d}{d\tau}({u_0}^{\beta}) = 0, \tag{B14}$$

with

$$u_\gamma^0(0) = 0 \quad \text{and} \quad \frac{du_\gamma^0}{d\tau}(0) = 0.$$

This problem can be solved using the variation of constants formula. One obtains after lengthy but straightforward computations (see the technical report [39]):

$$u_\gamma^0 = -u_0' \int_0^\tau \frac{d}{ds}(u_0^\beta) u_1 ds + u_1 \int_0^\tau \frac{d}{ds}(u_0^\beta) u_0' ds, \tag{B15}$$

where $u_0' = \frac{du_0}{d\tau}$, u_1 is the solution to

$$\frac{d^2 u_1}{d\tau^2} + \alpha u_0^{\alpha-1} u_1 = 0, \tag{B16}$$

$$u_1(T_0/2) = (\tilde{g} - u_M^\alpha)^{-1}, \quad \frac{du_1}{d\tau}(T_0/2) = 0, \tag{B17}$$

and $u_M = u_0(\frac{T_0}{2})$ satisfies (13) (hence $\tilde{g} - u_M^\alpha < 0$ in (B17)). Note that u_0' and u_1 are independent solutions to the homogeneous problem (B16).

Substitution of (B15) in (B13) yields after lengthy algebraic manipulations (see [39])

$$\frac{\partial \mathcal{I}}{\partial \gamma}(0, \tilde{g}) = -\beta \, \mathcal{I}_0 \, \mathcal{Q}_0, \tag{B18}$$

where $\mathcal{I}_0$ is given by (A3) and

$$\begin{aligned} \mathcal{Q}_0 &= -\beta^{-1} \int_0^{T_0/2} u_1 u_0^{\beta-1} [(\beta+\alpha) u_0^\alpha - \tilde{g}\beta] d\tau \\ &= \beta^{-1} \int_0^{T_0/2} \frac{u_1}{u_0'} \frac{d}{d\tau}(u_0^\beta u_0'') \, d\tau \end{aligned}$$

(the second identity follows from (9)). This integral can be further simplified using the fact that

$$\frac{d}{d\tau}\left(\frac{u_1}{u_0'}\right) = -\frac{1}{(u_0')^2} \tag{B19}$$

and integrating twice by parts (see [39]), which yields finally

$$\mathcal{Q}_0 = \int_0^{T_0/2} u_0^{\beta-1} d\tau. \tag{B20}$$

This integral can be rewritten in the form (40) by changing the integration variable ($\tau \to u_0$) and using (A4).

Now that $\frac{\partial \mathcal{I}}{\partial \gamma}(0, \tilde{g})$ has been computed with (B18)-(B20), substitution into (35) yields the squared restitution coefficient

$$e^2 = 1 - 2\beta \mathcal{I}_0 \gamma + 2\beta^2 \mathcal{I}_0 \mathcal{Q}_0 \gamma^2 + o(\gamma^2), \tag{B21}$$

where $\mathcal{I}_0, \mathcal{Q}_0 > 0$ are given in (A3), (B20). Dropping the $o(\gamma^2)$ remainder in (B21) and taking the square root, one obtains the following approximation of the CoR

$$e \approx \left(1 - 2\beta \mathcal{I}_0 \gamma + 2\beta^2 \mathcal{I}_0 \mathcal{Q}_0 \gamma^2\right)^{1/2}. \tag{B22}$$

For this approximation to be meaningful, it is necessary to have $1 - 2\beta \mathcal{I}_0 \gamma + 2\beta^2 \mathcal{I}_0 \mathcal{Q}_0 \gamma^2 \geq 0$, and we shall set $e = 0$ if this condition is not satisfied. This leads us to an approximation $e \approx e_+$ valid for $\gamma \approx 0$, where

$$e_+ = \max\left(1 - 2\beta \mathcal{I}_0 \gamma + 2\beta^2 \mathcal{I}_0 \mathcal{Q}_0 \gamma^2, 0\right)^{1/2}. \tag{B23}$$

Moreover, expanding the right side of (B22) at order 2 in γ yields the simplified approximation

$$e \approx 1 - \beta \mathcal{I}_0 \gamma + \beta^2 \mathcal{I}_0 (\mathcal{Q}_0 - \frac{1}{2}\mathcal{I}_0) \gamma^2 \tag{B24}$$

for $\gamma \approx 0$. We thus have another approximation $e \approx e_s$ at hand, given by

$$e_s = \max\left(1 - \beta \mathcal{I}_0 \gamma + \beta^2 \mathcal{I}_0 (\mathcal{Q}_0 - \frac{1}{2}\mathcal{I}_0) \gamma^2, 0\right). \tag{B25}$$

In numerical computations we observe that approximations (B22) and (B24) tend to overestimate the CoR, hence it is interesting to choose the smallest approximation. This leads us to consider

$$e \approx \min(e_+, e_s). \tag{B26}$$

In particular, if $1 - 2\beta \mathcal{I}_0 \gamma + 2\beta^2 \mathcal{I}_0 \mathcal{Q}_0 \gamma^2 \geq 0$ and (B24) is positive, (B26) corresponds to $e \approx e_s$ if

$$(\mathcal{Q}_0 - \frac{\mathcal{I}_0}{2}) \left(\beta(\mathcal{Q}_0 - \frac{\mathcal{I}_0}{2})\gamma - 2\right) \leq 0$$

and $e \approx e_+$ otherwise.

Appendix C Proof of Proposition 3

In this appendix we derive the approximation described in Proposition 3 for the integral $M_{\alpha,\beta}(\theta)$ defined in (51).

We first note that $M_{\alpha,\beta}(\theta)$ at $\theta = 0$ and $\theta = 1$ can be expressed in terms of Euler's Beta function

using (19), i.e. one has

$$M_{\alpha,\beta}(0) = \int_0^1 (1-x^\alpha)^{-1/2} x^{\beta-3/2} dx = \frac{1}{\alpha} \mathrm{B}\left(\frac{\beta-1/2}{\alpha}, \frac{1}{2}\right), \tag{C27}$$

$$M_{\alpha,\beta}(1) = \int_0^1 \left(1-x^{\alpha+1}\right)^{-1/2} x^{\beta-1} dx = \frac{1}{\alpha+1} \mathrm{B}\left(\frac{\beta}{\alpha+1}, \frac{1}{2}\right). \tag{C28}$$

In the general case, let us rewrite the integral $M_{\alpha,\beta}(\theta)$ as

$$M_{\alpha,\beta}(\theta) = \int_0^1 \left(x^{1-\theta} - x^{\alpha+1}\right)^{-1/2} h_{\alpha,\theta}(x) x^{\beta-1} dx, \tag{C29}$$

where

$$h_{\alpha,\theta}(x) = \left(\frac{x^{1-\theta} - x^{\alpha+1}}{\theta + (1-\theta)x - x^{\alpha+1}}\right)^{\frac{1}{2}} \quad \forall\, x \in [0,1) \tag{C30}$$

and $h_{\alpha,\theta}(1) = 1$. In order to approximate $M_{\alpha,\beta}(\theta)$, we will replace $h_{\alpha,\theta}(x)$ by an interpolation polynomial $p_n(x)$ of degree $\leq n$. This will provide an approximation of $M_{\alpha,\beta}(\theta)$ as a linear combination of Beta functions. Moreover, when $\theta = 0$ and $\theta = 1$ one has $h_{\alpha,\theta}(x) = 1$ for all $x \in (0,1]$ (leading to the explicit forms (C27) and (C28)), hence p_n will be equal to unity and the approximation will coincide with $M_{\alpha,\beta}(\theta)$.

To choose the interpolation points, one can notice that $h_{\alpha,\theta}(0) = 0$ for all $\theta \in (0,1)$, hence the convergence of $h_{\alpha,\theta}$ towards unity when $\theta \to 0$ or 1 is not uniform near $x = 0$. Consequently, it is useful to consider a fine mesh of interpolation points near $x = 0$. For this purpose, we extend $h_{\alpha,\theta}$ by symmetry over the interval $[0,2]$, defining

$$\tilde{h}_{\alpha,\theta}(x) = \begin{cases} h_{\alpha,\theta}(x) & \text{if } x \in [0,1], \\ h_{\alpha,\theta}(2-x) & \text{if } x \in [1,2], \end{cases} \tag{C31}$$

and consider the Chebyshev interpolation points over $[0,2]$:

$$x_k = \cos\left(\pi \frac{2k+1}{2n+2}\right) + 1, \quad 0 \leq k \leq n. \tag{C32}$$

We define p_n as the interpolation polynomial of $\tilde{h}_{\alpha,\theta}$ at $x_0, x_1, \ldots, x_n$ and perform the approximation

$$M_{\alpha,\beta}(\theta) \approx \int_0^1 \left(x^{1-\theta} - x^{\alpha+1}\right)^{-1/2} p_n(x)\, x^{\beta-1} dx. \tag{C33}$$

The interpolation polynomial can be conveniently expressed in the basis of Chebyshev polynomials, leading to

$$p_n(x) = \sum_{0 \leq j \leq n}{}' c_j T_j(x-1), \tag{C34}$$

where $\sum'$ denotes summation with first ($j = 0$) term halved, and $T_j(y) = \cos(j \arccos y)$ ($0 \leq j \leq n$) are the Chebyshev polynomials for $y \in [-1,1]$. Using a discrete orthogonality property of Chebyshev polynomials at Chebyshev nodes, one finds for $0 \leq j \leq n$ (see e.g. [45], chapter 6)

$$c_j = \frac{2}{n+1} \sum_{k=0}^{n} \tilde{h}_{\alpha,\theta}(x_k) \cos\left(j\pi \frac{2k+1}{2n+2}\right). \tag{C35}$$

Let us further assume n odd for simplicity. Thanks to the symmetry properties $x_{n-k} = 2 - x_k$ and $\tilde{h}_{\alpha,\theta}(x_{n-k}) = \tilde{h}_{\alpha,\theta}(x_k)$, the even coefficients c_{2p} in (C35) simplify to (55) and the odd coefficients c_{2p+1} vanish.

Now having obtained the interpolation polynomial (C34), we substitute its expression in the approximation (C33) of the integral $M_{\alpha,\beta}(\theta)$, which leads to

$$M_{\alpha,\beta}(\theta) \simeq \sum_{0 \leq j \leq n-1,\, j \text{ even}}{}' c_j\, a_{j,0}, \tag{C36}$$

with coefficients given by (55) and the case $k = 0$ of

$$a_{j,k} = \int_0^1 T_j(x-1) \left(1 - x^{\alpha+\theta}\right)^{-\frac{1}{2}} x^{\beta+\theta/2-3/2+k} dx. \tag{C37}$$

One can compute the coefficients $a_{j,k}$ by induction, given that

$$T_{j+2}(y) = 2y\, T_{j+1}(y) - T_j(y), \quad \text{for all } j \geq 0. \tag{C38}$$

Indeed, substituting (C38) in the definition of $a_{j+2,k}$, one obtains for all $j \geq 0$

$$a_{j+2,k} = 2(a_{j+1,k+1} - a_{j+1,k}) - a_{j,k}. \quad \text{(C39)}$$

Moreover, substituting $T_1(y) = y$ in the definition of $a_{1,k}$, we get

$$a_{1,k} = a_{0,k+1} - a_{0,k}. \quad \text{(C40)}$$

The recurrence is initiated with the values

$$a_{0,k} = \frac{1}{\alpha+\theta} \mathrm{B}\left(\frac{\beta + k - 1/2 + \theta/2}{\alpha+\theta}, \frac{1}{2}\right) \quad \text{(C41)}$$

for $0 \leq k \leq n-1$, which are obtained by substituting $T_0(y) = 1$ in the definition of $a_{0,k}$ and using (19). The recurrence procedure that determines coefficients $a_{j,k}$ for $0 \leq k \leq n-1-j$ is summarized in Table 1. One ends up with the values of $a_{0,0}, a_{2,0}, a_{4,0}, \ldots, a_{n-1,0}$ required to evaluate approximation (C36). Because of expression (C41) and the recurrence rule, the approximation (C36) consists of a linear combination of Beta functions.

Compliance with ethical standards

Conflict of Interest: The authors declare that they have no conflict of interest.

References

[1] Goldsmith, W.: Impact: The Theory and Physical Behavior of Colliding Solids. E. Arnold Publishers, London (1960)

[2] Routh, E.J.: An Elementary Treatise on the Dynamics of a System of Rigid Bodies. Macmillan, London (1877)

[3] Darboux, G.: Mémoire sur la théorie algébrique des forces quadratiques. Journal de Mathématiques Pures et Appliquées **19**, 347–396 (1874)

[4] Darboux, G.: Etude géométrique sur les percussions et le choc des corps. Bulletin des Sciences Mathématiques et Astronomiques **4**(1), 126–160 (1880)

[5] Brogliato, B.: Nonsmooth Mechanics. Models, Dynamics and Control, 3rd edn. Springer, Switzerland (2016)

[6] Nguyen, N.S., Brogliato, B.: Multiple Impacts in Dissipative Granular Chains. Lecture Notes in Applied and Computational Mechanics, vol. 72. Springer, Berlin Heidelberg (2014)

[7] Lee, J., Herrmann, H.J.: Angle of repose and angle of marginal stability: molecular dynamics of granular particles. J. Phys. A: Math. Gen. **26**, 373–383 (1993)

[8] Herbold, E.B., Nesterenko, V.F.: Shock wave structure in a strongly nonlinear lattice with viscous dissipation. Phys. Rev. E **75**, 021304 (2007)

[9] Alves, J., Peixinho, N., da Silva, M.T., Flores, P., H.M.Lankaranic: A comparative study of the viscoelastic constitutive models for frictionless contact interfaces in solids. Mechanism and Machine Theory **85**, 172–188 (2015)

[10] Corral, E., Moreno, R.G., García, M.G., Castejón, C.: Nonlinear phenomena of contact in multibody systems dynamics: a review. Nonlinear Dynamics **104**, 1269–1295 (2021)

[11] Tsuji, Y., Tanaka, T., Ishida, T.: Lagrangian numerical simulation of plug flow of cohesionless particles in a horizontal pipe. Powder Technology **71**(3), 239–250 (1992)

[12] Crook, A.: A study of some impacts between metal bodies by a piezoelectric method. Proc. Royal. Soc. A. Math. Phys. Eng. Sci. **212**(1110), 377–390 (1952)

[13] Džiugys, A., Peters, B.: An approach to simulate the motion of spherical and non-spherical fuel particles in combustion chambers. Granular Matter **3**(4), 231–266 (2001)

[14] Antonyuk, S., Heinrich, S., Tomas, J., Deen, N.G., Van Buijtenen, M.S., Kuipers, J.: Energy absorption during compression and

impact of dry elastic-plastic spherical granules. Granular Matter **12**(1), 15–47 (2010)

[15] Johnson, K.L.: Contact Mechanics. Cambridge University Press, Cambridge (1985)

[16] Brake, M.R.: An analytical elastic-plastic contact model with strain hardening and frictional effects for normal and oblique impacts. Int. J. Solids Struct. **62**, 104–123 (2015)

[17] Xiong, X., Kikuuwe, R., Yamamoto, M.: A multiscale friction model described by continuous differential equations. Tribol. Letters **51**, 513–523 (2013)

[18] Bastien, J., Lamarque, C.H.: Persoz' gephyroidal model model described by a maximal monotone differential inclusion. Arch. Appl. Mechanics **78**(5), 393–407 (2008)

[19] Bastien, J., Michon, G., Manin, L., Dufour, R.: An analysis of the modified Dahl and Masing models: application to a belt tensioner. Journal of Sound and Vibration **302**, 841–864 (2007)

[20] Maugis, D.: Contact, Adhesion and Rupture of Elastic Solids. Solid-State Sciences. Springer, Heidelberg (2000)

[21] Stronge, W.J.: Rigid body collision with friction. Proc. Royal Soc. Lond. A **431**(1881), 169–181 (1990)

[22] Stronge, W.J.: Friction in collisions: Resolution of a paradox. J. Applied Phys. **69**(2), 610–612 (1991)

[23] Stronge, W.J.: Smooth dynamics of oblique impacts with friction. Int. J. Impact Eng. **51**, 36–49 (2013)

[24] Stronge, W.J.: Energetically consistent calculations for oblique impacts in unbalanced systems with friction. ASME J. Applied Mechanics **82**(8), 081003 (2015)

[25] Simon, R.: The development of a mathematical tool for evaluating golf club performance. Proceedings of ASME Design Engineering Congress, New York City, USA (1967)

[26] Hunt, K.H., Crossley, F.R.E.: Coefficient of restitution interpreted as damping in vibroimpact. ASME Journal of Applied Mechanics **42**(2), 440–445 (1975)

[27] Kuwabara, G., Kono, K.: Restitution in a collision between two spheres. Japan. J. Appl. Phys. **26**(8), 1230–1233 (1987)

[28] Falcon, E., Laroche, C., Fauve, S., Coste, C.: Behavior of one inelastic ball bouncing repeatedly off the ground. Eur. Phys. J. B **3**, 45–57 (1998)

[29] Shi, P.: The restitution coefficient for a linear elastic rod. Mathematical and Computer Modelling **28**(4-8), 427–435 (1998)

[30] Shen, Y., Xiang, D., Wang, X., Jiang, L., Wei, Y.: A contact force model considering constant external forces for impact analysis in multibody dynamics. Multibody System Dynamics **44**(4), 397–419 (2018)

[31] Carvalho, A.S., Martins, J.M.: Exact restitution and generalizations for the Hunt-Crossley contact model. Mechanism and Machine Theory **139**, 174–194 (2019)

[32] Schwager, T., Pöschel, T.: Coefficient of normal restitution of viscous particles and cooling rate of granular gases. Physical Review E **57**(1), 650–654 (1998)

[33] Ramirez, R., Pöschel, T., Brilliantov, N.V., Schwager, T.: Coefficient of restitution of colliding viscoelastic spheres. Physical Review E **60**(4), 4465–4472 (1999)

[34] Müller, P., Pöschel, T.: Collision of viscoelastic spheres: compact expressions for the coefficient of normal restitution. Physical Review E **84**(2) (2011)

[35] Schwager, T., Pöschel, T.: Coefficient of restitution for viscoelastic spheres: The effect of delayed recovery. Physical Review E **78**(5), 051304 (2008)

[36] Brilliantov, N.V., Spahn, F., Hertzsch, J.M., Pöschel, T.: The collision of particles in granular systems. Phys. A **231**, 417–424 (1996)

[37] Brilliantov, N.V., Spahn, F., Hertzsch, J.M., Pöschel, T.: Model for collisions in granular gases. Physical Review E **53**(5), 5382–5392 (1996)

[38] Brilliantov, N.V., Pimenova, A.V., Goldobin, D.S.: A dissipative force between colliding viscoelastic bodies: Rigorous approach. EPL (Europhysics Letters) **109**(1) (2015)

[39] Chatterjee, A., James, G., Brogliato, B.: Approximate analytical coefficient of restitution formulation for single bead impact with external load, using nonlinear visco-elastic models. Research Report hal-03462750, INRIA (December 2021). https://hal.inria.fr/hal-03462750

[40] James, G.: Traveling fronts in dissipative granular chains and nonlinear lattices. Nonlinearity **34**(3), 1758 (2021)

[41] James, G., Vorotnikov, K., Brogliato, B.: Kuwabara-Kono numerical dissipation: a new method to simulate granular matter. IMA Journal of Applied Mathematics **85**(1), 27–66 (2020)

[42] Falcon, E.: Comportements dynamiques associés au contact de Hertz : processus collectifs de collision et propagation d'ondes solitaires dans les milieux granulaires. PhD thesis, Université Claude Bernard Lyon I (1997)

[43] Zhao, Z., Liu, C., Brogliato, B.: Energy dissipation and dispersion effects in granular media. Physical Review E **78**(3), 031307 (2008)

[44] Chatterjee, A., James, G., Brogliato, B.: Approx-ViscoElastic-CoR. GitHub (2021). https://github.com/ChattAbhi/Approx-ViscoElastic-CoR.git/

[45] Mason, J.C., Handscomb, D.C.: Chebyshev Polynomials. Chapman & Hall/CRC, Boca Raton (2003)